# Using a heated column experiment to investigate the long-term effects of thermal recovery operations on the release, mobilization, and attenuation of arsenic in groundwater

by

Cassandra Stead

A thesis submitted to the Faculty of Graduate and Postdoctoral Affairs in partial fulfillment of the requirements for the degree of

Master of Science

In

Earth Sciences

Carleton University
Ottawa, Ontario

# Abstract

Steam assisted gravity drainage is a form of thermal recovery technology used for unconventional oil. It can result in the heating of surrounding sediments and associated porewater and has the potential to mobilize otherwise immobile groundwater contaminants, such as arsenic. The current study was conducted to continue with the analysis of geochemical reactions within a column to gain a better understanding of the long-term effects of thermal recovery operations on groundwater contamination, with an emphasis on arsenic. A temperature range of 50 °C to 90 °C was implemented within a heated section of the column to mimic thermal influence on an aquifer adjacent to a steam assisted gravity drainage well. During the year-long study, aqueous concentrations of silica, arsenic, aluminum, titanium, and zinc were found to increase within the heated section of the column. This suggests that thermal recovery operations do have the potential to mobilize contaminants in groundwater.

# Acknowledgements

I would like to express my deep gratitude to everyone who helped make this thesis possible. First and foremost, I would like to thank my supervisor, Dr. Richard Amos. I am truly grateful for his very patient guidance and genuine support. For sharing their insights on this project, I would like to thank Dr. Paul Gammon, Dr. Tom Al, Dr. Jon Fennell, and Dr. George Dix. For the preparation of my thin sections I would like to thank Tim Mount. I would like to further thank Tim for the invaluable knowledge he passed down to me while working for him at the sample preparation laboratory. For the prompt and quality geochemical analyses of various samples I would like to thank Dr. Nimal De Silva, Dr. Maryam Shahabi Far, and Lilianne Pagé. Special thanks are in order to Andrew Craig, for his hard work on the preliminary experiments of this project, and to Andrew Hicks, for his help with the set-up of the column and sample collection. I would also like to thank my friends and family, especially my parents, for their ongoing support in everything that I choose to pursue. Lastly, I would like to acknowledge my daughter, whose heart is so big and full of understanding. Thank you for your pure love.

# Table of Contents

Abstract ..... ii

Acknowledgements ..... iii

Table of Contents ..... iv

List of Figures ..... vi

1.0 Introduction ..... 1

1.1 Background Information ..... 1

1.2 Objectives and Purpose ..... 4

2.0 Relative Information ..... 6

2.1 Geology and Hydrogeology of the Oil Sands ..... 6

2.2 Arsenic in the Oil Sands In-Situ Area ..... 9

2.2.1 Occurrence and Geochemistry of Arsenic ..... 9

2.2.2 Impact of Thermal Recovery Operations on Arsenic ..... 12

2.3 The Role of Temperature in Hydrogeochemical Processes ..... 14

3.0 Methods and Materials ..... 17

3.1 Experiment Design ..... 17

3.2 Sampling Regime ..... 20

3.3 Sediment Characterization ..... 23

4.0 Results ..... 27

4.1 Conditions Within the Column ..... 27

4.1.1 Physical Conditions ..... 27

4.1.2 Porewater Geochemistry ..... 29

4.1.3 Sediment Characterization ..... 46

5.0 Discussion ..... 55

5.1 Unheated Study ..... 55

5.2 Heated Study ..... 57

5.3 Changes in Sediment Composition ..... 62

5.4 The Release, Mobilization, and Attenuation of Arsenic ..... 66

6.0 Conclusion ..... 69

7.0 References ..... 72

# List of Figures

Figure 1.1 Oil Sands deposit area in Alberta. ..... 3

Figure 1.2 Schematic diagram of a typical SAGD operation ..... 4

Figure 3.1 Schematic design of the column set-up ..... 20

Figure 3.2 Location of collected sediment ..... 26

Figure 3.3 Schematic depicting location of samples collected from the column ..... 26

Figure 4.1 Average temperatures along the length of the column ..... 28

Figure 4.2 Flow rate within the column. ..... 28

Figure 4.3 pH (a), alkalinity (b), Eh (c), DO (d), conductivity (e), sulphate (f), sulphide (g), and ferrous iron (h) ..... 42

Figure 4.4 Phosphorous (a), silica (b), calcium (c), sodium (d), potassium (e), and magnesium (f). ..... 43

Figure 4.5 Arsenic (a), Aluminum (b), titanium (c), zinc (d), total iron (e), copper (f), manganese (g), and nickel (h) ..... 44

Figure 4.6 Phase diagrams of iron (a), arsenic (b), and sulphate (c). ..... 45

Figure 4.7 XRD data ..... 51

Figure 4.8 Microprobe images showing microcline (a), albite (b), and quartz (c) as well as a quartz grain exhibiting pitting (d). ..... 52

Figure 4.9 Microprobe images showing an oxide with iron-rich (a) and titanium-rich (b) phases as well as biotite (c). ..... 52

Figure 4.10 Microprobe images showing pyrite grains ..... 53

Figure 4.11 Types of phosphates found within the column including apatite (a), iron-rich (b), and aluminum-rich (c). ..... 53

Figure 4.12 SI for quartz (a), microcline (b), albite (c), muscovite (d), calcite (e), ferrihydrite (f), gibbsite (g), hydroxyapatite (h), strengite (i), vivianite (j), gypsum (k), and $O_{2(g)}$ (l) ..... 54

# 1.0 Introduction

## 1.1 Background Information

Canada, for better or for worse, has an economy that is tied heavily to oil. It is the fourth largest producer and fourth largest exporter of oil in the world (Natural Resources Canada [NRC], 2018) and 98% of Canada's proven oil reserves are in the Oil Sands, located in northern Alberta (Figure 1.1; Government of Alberta [GOA], 2019). However, only 20% of this resource is recoverable using conventional surface mining. The remaining 80% is deep within the earth's surface (greater than 70 meters) and must be recovered using in-situ methods (NRC, 2018; Canadian Association of Petroleum Producers [CAPP], 2018). Often, these methods involve thermal recovery technology which employs heating techniques to change the properties of the oil, allowing for its recovery. One such method of thermal technology includes steam assisted gravity drainage (SAGD).

SAGD involves drilling pairs of horizontal wells from central well pads into the oil reservoir (Figure 1.2). High-temperature steam injection through the upper well (~200 °C; Javed & Siddique, 2016) heats the bitumen to a temperature at which it can flow by gravity into the lower wells. The resulting oil and condensed steam mixture are then pumped from the lower wells to a processing plant where the oil is separated from the mixture and treated (GOA, 2017). The only surface development involves the construction of the well pad and wells, and therefore the technology is thought to have a smaller environmental footprint compared to open-pit mining. However, this process does not come without side-effects.

There has been, and still is, public concern that the application of heat may influence the release of naturally occurring contaminants in aquifers that overly the oil reservoir. During the high temperature steam injection used to heat the oil, heat radiates away from the steam injection wells to surrounding sediment and associated porewater, which has the potential to mobilize otherwise immobile constituents, such as arsenic (As; Alberta Geological Survey, 2002). Thermal recovery operations have been linked as an anthropogenic source of arsenic in groundwater in Alberta (Fennell, 2008; Waterline Inc., 2011; Javed & Siddique, 2016). There is limited knowledge as to why this occurs, and the mechanisms of release, mobilization, and attenuation of arsenic in groundwater is an issue that needs to be addressed and studied in greater detail.

Inorganic arsenic, being very toxic, is the most significant chemical contaminant in drinking-water globally and the greatest threat to public health from arsenic originates from contaminated groundwater (World Health Organization [WHO], 2011). The devastation that can be caused by this toxin has most-notably been witnessed in Bangladesh, where groundwaters were found to have levels of arsenic above 0.05 mg $L^{-1}$ (Smith, Lingas, & Rahman, 2000). In Canada, about one quarter of Canadians obtain their drinking water from groundwater (Government of Canada [GOC], 2013) and the occurrence of groundwater with arsenic concentrations in excess of the current maximum acceptable concentration (MAC) of 0.01 mg $L^{-1}$ for drinking water in Canada (Health Canada, 2006) has been noted in Newfoundland and Labrador, Prince Edward Island, Nova Scotia, New Brunswick, Québec, Manitoba, Saskatchewan, Alberta, and British Columbia (Canadian Water Network [CWN], 2015).

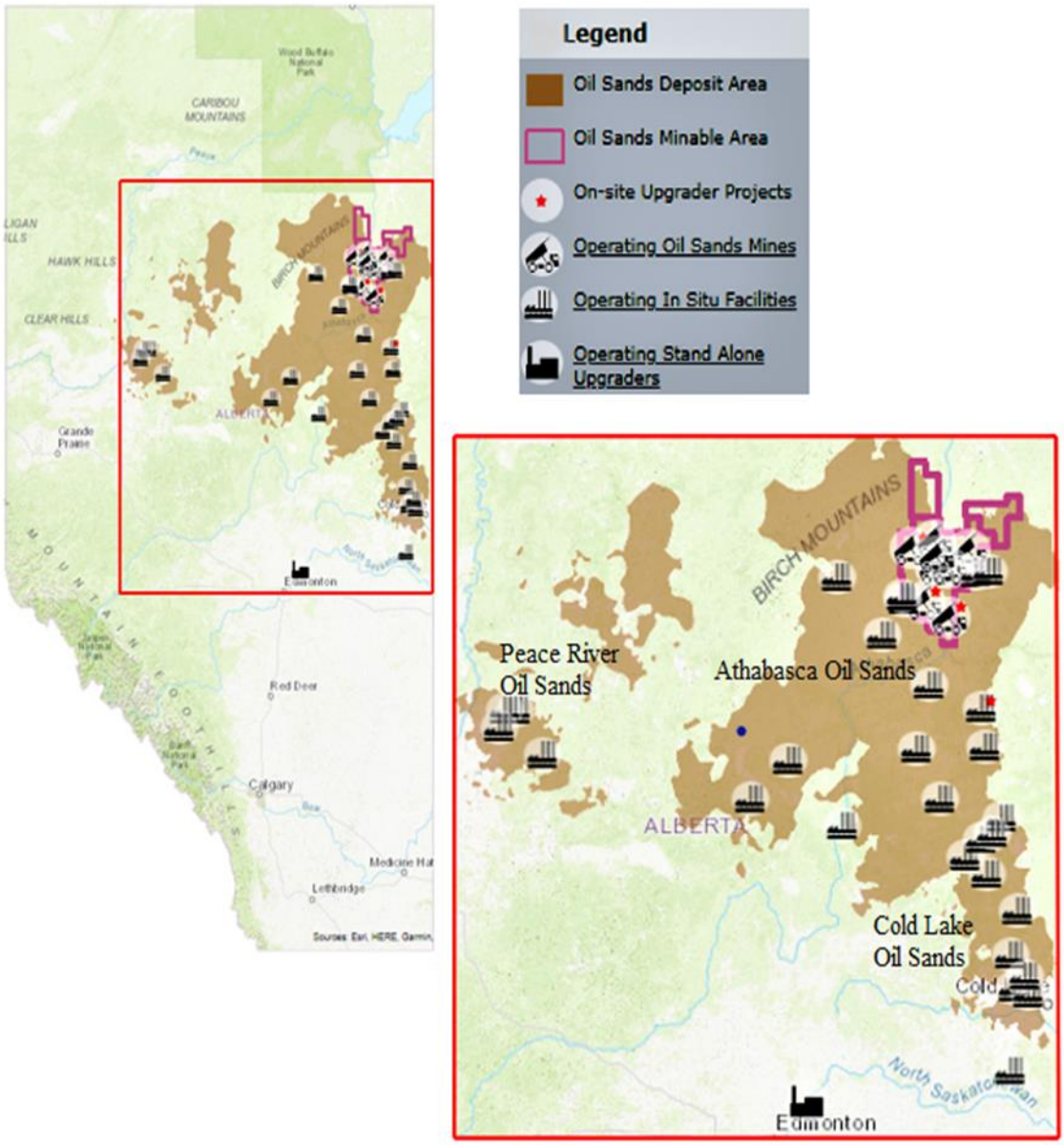


*Figure 1.1 Oil Sands deposit area in Alberta, highlighting operating mines and in-situ facilities (created based on data from GOA, 2019).*

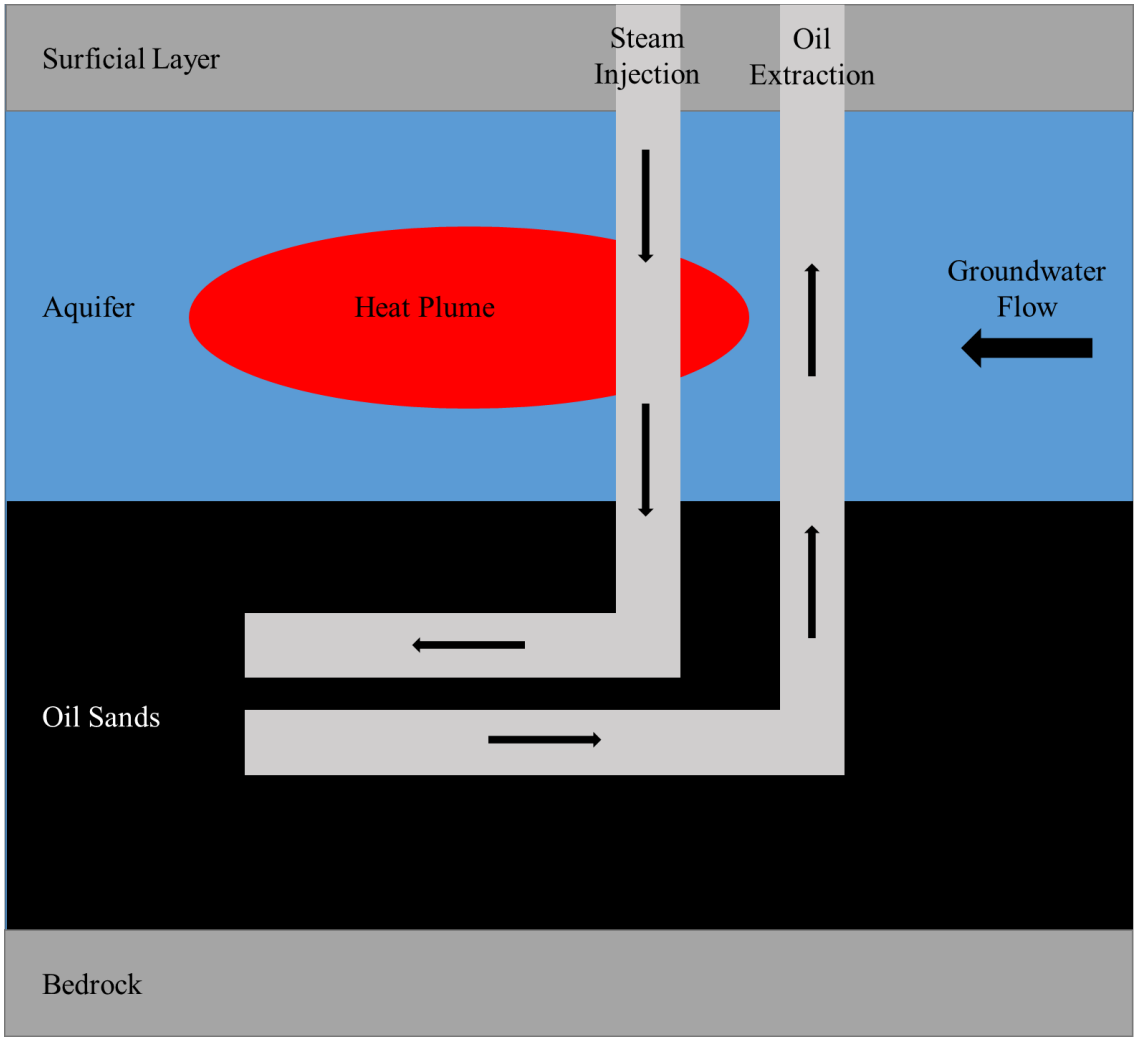


*Figure 1.2 Schematic diagram of a typical SAGD operation, showing resulting heat plume due to high-temperature steam injection.*

## 1.2 Objectives and Purpose

Collection of good baseline data and fundamental research into the controls on the distribution and mobility of naturally occurring contaminants, such as arsenic, is vital in understanding the impact of thermal recovery operations on groundwater quality. Few field and laboratory studies have been conducted that investigate this issue and the laboratory studies have consisted of controlled batch experiments (Fennell, 2008; Javed

& Siddique, 2016). Batch experiments are often useful for determining thermodynamic or kinetic parameters however, batch tests have the disadvantage of being conducted under conditions often not representative of conditions observed in the field. Specifically, they are carried out under static conditions without advective flow (Porro, Newman, & Dunnivant, 2000). Column tests have the advantage of being conducted under conditions more closely approximating those observed in the field, specifically including advective and dispersive transport. These types of experiments can provide an understanding of the coupled hydrological and reactive transport mechanisms responsible for producing observed effects from thermal recovery operations.

This research project began with the construction of a column in 2015, followed by characterization of chemical and physical properties of the column and analysis of initial geochemical reactions within the column. This was done at Carleton University as a master's thesis (Craig, 2017). The current study was meant to continue with the analysis of geochemical reactions within the column to gain a thorough understanding of the geochemical and physical transport processes affecting water-rock interactions in thermally impacted aquifers and the influence these processes have on contaminants, especially the release, transport and attenuation of arsenic. This is to gain a better understanding of the long-term effects of thermal recovery operations on groundwater contamination. Particular interest was placed on arsenic because of its toxicity and the observation that arsenic is released from heating aquifer sediment in Alberta (Fennell, 2008; Waterline Inc., 2011; Javed & Siddique, 2016).

# 2.0 Relative Information

## 2.1 Geology and Hydrogeology of the Oil Sands

The geology of the Athabasca Oil Sands (In Situ) region of northeast Alberta has been described in great detail by Parks and Andriashek (2002). The geological landscape of the area exhibits remnants of buried fluvial channels with infill of varied origin, separated by two main unconformities- the Pre-Cretaceous and Pre-Quaternary Unconformities. The Pre-Cretaceous Unconformity is a buried surface of extensive sub-areal erosion marking the top of Devonian strata. Sitting directly atop the unconformity is the Lower Cretaceous McMurray Formation, which hosts the bitumen as well as substantial gas resources. In addition, it is a major regional aquifer. Overtop of the McMurray are the sandstones and shales of the Lower Cretaceous Clearwater and Grand Rapids formations, which also host natural gas deposits. These formations, as well as the others that lie beneath the Pre-Quaternary Unconformity, are characterized by broad fluvial channels with infill attributed to the cyclic regression and advance of the sea, which was to the north at the time of deposition.

Parks and Andriashek (2002) also describe the formations above the Pre-Quaternary unconformity, including the Empress Formation, which is thought to be the largest aquifer overlaying the oil-bearing formations and marks the beginning of glacial activity. The infill of the buried fluvial valleys in the Tertiary-Quaternary formations is attributed to cyclic glacial advance and retreat, rather than the sea. In this region, the buried bedrock channels can be grouped as either pre-glacial or glacial. Pre-glacial fill is composed primarily of metaquartzite and sandstone or chert derived from Cordilleran rock sources,

from local Cretaceous bedrock sources, or from recycled gravel that was deposited during an earlier stage in the erosion of the bedrock landscape, while glacial fill is characterized as granites and gneissic clasts from the Canadian Shield Deposits.

These buried channels create the significant aquifers which surround, and even in some cases contain, oil-bearing formations. Of great importance are the bedrock interfluves between major channels within the lowlands of the area. Parks and Andriashek (2002) suggest that interfluves may increase the potential for expansion of heat plumes from SAGD operations. These interfluves, composed of glacial fill and with a higher hydraulic conductivity than surrounding shales, can act as bridges between oil reservoirs and aquifers that may lay above capping aquitards potentially resulting in a transfer of heat between aquifers.

The hydrogeology of the region is described in various references, including Parks and Andriashek (2002), Lemay, (2003), Ozoray, (1974), Hitchon et al., (1989), Bachu et al., (1993), Stein et al., (1993), Stewart, (2003), and during projects such as the Devon ARL Corporation [Devon] (2006) and Canadian Natural Resources Limited [CNRL] Kirby (2007) projects. The Pre-Cambrian base is overlain by Devonian carbonates; a saline aquifer. The Cretaceous strata overlying the Devonian strata, including the McMurray formation, have been determined to include regionally extensive saline and non-saline sandstone aquifers, while the Tertiary-Quaternary sediments, including the Empress Formation, consist of a non-saline, layered aquifer/aquitard assemblage. Within buried valleys, sub-horizontal flow is directed along the axis of the channel thalweg, such as within the Wiau Channel within the Empress Formation (Channel Sand aquifer).

Recharge generally occurs in locations of higher elevation, or uplands, while discharge sites typically include the lowlands, rivers and lakes. Specifically, the Athabasca River Valley is thought to receive discharge from the Channel Sand aquifer.

Parks and Andriashek (2002) found that conductivity of the Empress aquifers ranged from 7 x 10-6 m $s^{-1}$ to 7 x 10-4 m $s^{-1}$. During the CNRL Kirby (2007) project, hydraulic response testing in the Empress Formation yielded a hydraulic conductivity range of $10^{-6}$ to $10^{-4}$ m $s^{-1}$, falling within the range described by Parks & Andriashek (2002). However, there were some areas where hydraulic conductivity in the Empress Formation were found to be as high as $10^{-2}$ m $s^{-1}$ during the CNRL Kirby (2007) Project and Lemay (2003), also suggests that flow velocities within these aquifers can change within the same area due to sediment heterogeneities in conjunction with cross formational flow.

The groundwater geochemistry of the region varies greatly depending on sediment lithology. In general, the reported groundwater quality parameters during the conductance of the Empress Formation Source Water Exploration Program (EFSWEP) by Waterline Inc. (2007) met the Guidelines for Canadian Drinking Water Quality (GCDWQ) with the exception for occasional exceedances of pH, sodium (Na), arsenic, iron (Fe) and manganese (Mn). Lemay (2003) found that primary constituents of total dissolved solids in the groundwater of the area are sodium, magnesium (Mg), calcium (Ca), bicarbonate ($HCO_3$), and sulphate ($SO_4$) ions. The Empress Formation is described as having calcium/sodium-bicarbonate type water with TDS concentrations in the range of 466-667 mg $L^{-1}$ (Devon, 2006).

## 2.2 Arsenic in the Oil Sands In-Situ Area

### 2.2.1 Occurrence and Geochemistry of Arsenic

In natural water, arsenic is generally present only in the $As^{5+}$ (arsenate) and/or $As^{3+}$ (arsenite) states as an oxyanion with the general forms $H_nAsO_4^{3-n}$ and $H_nAsO_3^{3-n}$, respectively (Welch, Lico, & Hughes, 1988). The prevalence of each arsenic species is highly dependent on pH and Eh. Under oxidizing conditions arsenate ($As^{5+}$) is dominant and under reducing conditions arsenite ($As^{3+}$) is dominant (Smedley & Kinniburgh, 2002). Oxyanion speciation and mobility of both oxidation states exhibit a strong dependence on pH. Arsenate is less mobile than arsenite (Lemay, 2003) but, is usually less prevalent in groundwater due to typically reducing conditions (Waterline Inc., 2011). Oxyanions of arsenate also tend to become less strongly sorbed as pH increases (Dzombak & Morel, 1990b), even at near-neutral pH values (Smedley & Kinniburgh, 2002).

Because of its ionic radii in both the arsenate and arsenite forms, arsenic can substitute for ions of silica ($Si^{4+}$), aluminum ($Al^{3+}$), ferric iron ($Fe^{3+}$), and titanium ($Ti^{4+}$), as well as sulphur (S) in numerous minerals (Smedley & Kinniburgh, 2002). Sources of arsenic are varied and include anthropogenic sources and minerals such as, arsenates, sulphides, sulphates, phosphates, arsenides, arsenites, oxides and native arsenic (Boyle & Jonasson, 1973; Lemay, 2003). Arsenic is often naturally enriched in specific minerals including pyrite ($FeS_2$), arsenopyrite (FeAsS), enargite ($Cu_3AsS_4$), scorodite ($FeAsO_4 \cdot 2H_2O$) and annabergite ($Ni_3(AsO_4)_2$; Boyle & Jonasson, 1973). Furthermore, shale of marine origin often contains elevated levels of arsenic that is concentrated in sulphide minerals (Muloin

& Dudas, 2011).

Weathering of these arsenic-bearing minerals under natural conditions can mobilize arsenic from soil and sediment to the aquatic environment (Smedley & Kinniburgh, 2002; Muloin & Dudas, 2011). Specific processes that can result in the release of arsenic into the groundwater system can include arsenic-bearing mineral dissolution, desorption of arsenic from soil and/or carbonate material or iron, aluminum, and/or manganese oxides/hydroxides, chemical transformation of arsenic through redox or other processes, ion exchange between arsenic and other elements, release of arsenic through biological activity, release of arsenic through anthropogenic activity, and/or wet or dry deposition of atmospheric arsenic (Lemay, 2003).

Arsenic is present naturally in Alberta. Parks & Andriashek, (2002), during their study of the Athabasca Oil Sands area, found that arsenic was, in various core samples, as high as 40 mg $kg^{-1}$ in samples of till. High arsenic values were observed to increase dramatically in the buried weathered oxidized profiles found within the till, which became progressively higher toward the bedrock contact, or with depth. High arsenic concentrations were notably found in the Lea Park Formation claystone. The same was found in a study by Javed et al., (2014) which was also conducted in the Athabasca Oil Sands area, where high arsenic concentrations were also found in the claystone of the Lea Park Formation- as high as 32 mg $kg^{-1}$, compared to average arsenic concentrations of ~5 mg $kg^{-1}$.

Arsenic in the groundwater may correlate to lithology and redox. A study was conducted by Lemay (2003) shortly after Parks and Andriashek (2002) in the same area, which

investigated groundwater geochemistry. In this study, aqueous samples were collected from Quaternary drift and buried channel aquifers in the Athabasca Oil Sands area to determine arsenic concentrations in the groundwater. Lemay (2003) found only ~19 % of the groundwater samples to have arsenic concentrations in exceedance to the MAC and that at the average aquifer temperature and redox conditions observed, the dominate arsenic species in the area would be arsenate. Since the majority of the samples had arsenic concentrations below the MAC, it was suggested that some mechanism must not allow it to enter solution, such as that Eh-pH conditions may not be conducive to the release of arsenic, or just that arsenic was present but, at concentrations below the detection limit.

A more recent study by Moncur et al. (2015) included a survey of water wells sampled for arsenic in the Cold Lake Beaver River (CLBR) basin within the Oil Sands. In this study, 50 % of the wells contained arsenic concentrations exceeding drinking water guidelines. It was suggested that higher arsenic concentrations in groundwater were associated with reducing conditions and that arsenite was the dominant species, contrary to the findings of Lemay (2003). This may be reflective of the sensitivity of arsenic speciation on lithology and redox. Furthermore, Moncur et al. (2015) found that the majority of groundwater samples were undersaturated with respect to ferrihydrite ($5Fe_2O_3 \cdot 9H_2O$), suggesting that reductive dissolution of iron oxides/hydroxides may be the source of some arsenic in groundwater in the area. This is in agreement with the speculations by Javed et al., (2014).

### 2.2.2 Impact of Thermal Recovery Operations on Arsenic

After development and further expansions began for In-Situ recovery of bitumen in the Oil Sands area, the concern regarding the potential effect of thermal heating on arsenic release and mobilization, and water quality in general, was raised. Fennell (2008) investigated the impact that thermal heating was having on arsenic concentrations in the field. The study included tests to characterize the Muriel Lake aquifer within the Cold Lake Oil Sands region and monitor temporal changes in temperature and the resulting geochemical changes. Fennell (2008) observed comparatively large temperature increases in profiles for each well. It was concluded that this was a direct indication of a nearby heat source.

Fennell (2008) suggested heat was being conveyed by the groundwater moving within the various aquifer intervals beneath the study area and the obvious source of heat was from active Cyclic Steam Simulation (CSS) pads, a technology similar to SAGD. A pattern of elevated median arsenic values correlated to elevated temperature conditions was apparent, indicating an effect from localized heating. Wells downgradient (15-55 m) of the CSS pad showed elevated arsenic concentrations relative to background concentrations, ranging from 0.027 mg $L^{-1}$ to 0.050 mg $L^{-1}$. Similarly, Javed and Siddique (2016) investigated thermal heating influence on arsenic and other metal(loids) in groundwater. Their study confirmed the presence of elevated arsenic in aquifers in close proximity to in-situ oil sands extraction in the Cold Lake region, attributed to heat propagated from hot injection wells altering physicochemical properties of the surrounding sediments and associated porewater.

Along with the field study, Fennell (2008) completed experiments in the laboratory to investigate effects of aquifer heating on groundwater chemistry, with great emphasis on arsenic. Sediments collected from the Muriel Lake Formation in the Cold Lake region were subjected to controlled laboratory experiments to assess arsenic release at increasing temperatures. Fennell found that release occurred at, or near, 50 ºC. In a similar way, a laboratory experiment by Javed and Siddique (2016) found that heat application to aquifer and fractured sediments from various formations, also from the Cold Lake Oil Sands region, released arsenic in the porewater (0.5−6.6 mg $L^{-1}$). They found that heat application altered arsenic distribution in the sediments, releasing arsenic from exchange surfaces and amorphous iron oxides to the soluble arsenic fraction.

The Canadian Natural Primrose In-Situ Oil Sands project investigated thermal impact on arsenic release and mobility, focusing on the Empress Formation beneath a steam injection well pad within the Cold Lake Oil Sands region (CNRL, 2006). A thermal plume formed by advective transport was found to extend approximately 350 m down-gradient from the well pad. A resulting dissolved-arsenic plume was found to extend approximately 360 m from the well pad, generally coinciding with the edge of the thermal plume, implying that there is a direct relationship between elevated temperature and dissolved arsenic concentration. The plume was characterized by higher concentrations of arsenic and sulphate, which was suggested to be a result of sulphide dissolution and oxidation. It was concluded that thermally increased arsenic concentrations may develop in the Empress Formation and in the aquifers within the undifferentiated Quaternary sediments.

## 2.3 The Role of Temperature in Hydrogeochemical Processes

Concentrations of arsenic in groundwater depend on mineral-water interactions, specifically the thermodynamics of mineral solubility and equilibria. Fundamental to any description of equilibria and understanding chemical processes which occur in groundwater is the *law of mass action* which can be described using the equilibrium constant, K (Appelo & Postma, 2005). For the general mass balance equations;

$$aA_{(s)} \rightleftharpoons bB_{(aq)} + cC_{(aq)} \quad (2.1)$$

$$K = [B]^b[C]^c \quad (2.2)$$

the bracketed upper-case letters represent the activity of each compound and the lower-case letters represent the respective stoichiometric coefficients. The reactant in this case is a solid, which is considered to have an activity of one and, therefore, is not represented in equation 2.2.

The saturation index, SI, can then be used to determine saturation states of any mineral and is calculated by;

$$SI = log\ (IAP/K) \quad (2.3)$$

where IAP describes the activities of aqueous compounds in a sample, rather than at equilibrium, and is calculated as all mass balance equations, substituting K for IAP. When SI = 0, there is equilibrium between the mineral and solution; when SI < 0 the solution is undersaturated with respect to the mineral and the mineral will have the tendency to dissolve; when SI > 0 the solution is supersaturated with respect to the mineral and the mineral will have the tendency to precipitate. In natural conditions groundwater is often out of equilibrium and the saturation state is used to determine

which direction chemical reactions are likely proceeding in.

However, mass action constants (i.e. K) depend on temperature (Appelo & Postma, 2005). This temperature dependency can be described by the Van't Hoff equation;

$$\frac{dlnK}{dT} = \frac{\triangle H_r}{RT^2} \qquad (2.4)$$

where $\triangle H_r$ is the reaction enthalpy, $R$ is the gas constant ($8.314 \times 10^{-3}$ kJ mol$^{-1}$ deg$^{-1}$), and $T$ is the absolute temperature in Kelvins. Reactions that result in a loss of heat from the system to the surroundings are considered exothermic (negative $\triangle H_r$), whereas reactions that result in absorption of heat by the system from the surroundings are considered endothermic (positive $\triangle H_r$). Furthermore, K decreases with increasing temperature for exothermic reactions and increases with increasing temperature for endothermic ones. In this way, temperature has the capacity to affect adsorption of contaminants by influencing the solubility and/or transformation of known adsorbents such as, iron oxides/hydroxides (Das, Hendry, & Essilfie-Dughan, 2011). Since arsenic is often controlled by surface adsorption, the dissociation/dissolution of adsorbents could impact its release and mobility in a system.

Thermodynamics predicts whether dissolution or precipitation is favourable, while reaction kinetics are used to describe the rate of the reaction; the change of concentration of a compound in time (Appelo & Postma, 2005). Reaction rates are determined experimentally and are described in terms of the relationship to the reactants, such as;

$$rate = k(A)^a \qquad (2.5)$$

where $k$ is the rate constant and $a$ is the reaction order with respect to A. As a general rule, the rate at which a chemical reaction proceeds doubles for every 10 °C increase in

temperature (Langmuir, 1997). An example is the influence of temperature on pH. As temperature increases, the rate of dissociation of water molecules to hydrogen and hydroxide ions increases. The relationship between rate and temperature is described in the Arrhenius equation;

$$k = A * exp\left[\frac{-E_a}{RT}\right] \qquad (2.6)$$

where A is the pre-exponential factor (same units as k) and $E_a$ is the activation energy (kJ $mol^{-1}$). As temperature increases so too will k and therefore, reaction rate increases with temperature.

# 3.0 Methods and Materials

## 3.1 Experiment Design

In this study, a heated column experiment was conducted to characterize and compare the effects of high temperature (50-90 °C) on groundwater contaminants, especially arsenic. Overall, the experiment was designed to mimic a fully saturated aquifer unit in contact with an in-situ thermal recovery well; accomplished by using aquifer sediments collected from the Athabasca Oil Sands (In-Situ) area in Alberta and the experiment was conducted entirely in an anaerobic chamber. The duration of the experiment was from June 18, 2017 to June 28, 2018. Samples were collected in two parts; from June 18-August 18, 2017 (Craig, 2017) and from October 30-June 28, 2018.

The heated experiment was preceded by a background, or unheated study, where the column was not heated (Craig, 2017). This study was conducted for four weeks from May 4-June 16, 2017 and samples were collected one day each week, for a total of four sampling days during the unheated study. On all plots presented in this text, the unheated experiment is denoted as U5, U12, U19, and U26. The heated study is denoted as days 5-375 on all plots presented in this text. During the heated study, the column was heated from 50-90 °C. This temperature range was implemented as it was found that it did not produce a phase change within the column (Craig, 2017), and because SAGD field observations have shown that temperatures reach approximately 100 °C in the aquifer units adjacent to the steam injection well (Giraldo & MacMillan, 2016).

The column set-up used during the study by Craig (2017) was used throughout the

duration of this project (Figure 3.1). This set up involved a polytetrafluoroethylene (PTFE) column enclosed with PTFE threaded end caps. PTFE is stable at temperatures of up to 200 °C and was used as the column material for its enhanced thermal tolerance. A horizontal column alignment was implemented to reduce density-driven mixing effects. The column had overall dimensions of 3.00 m in length and a 0.05 m inner diameter. Inflow water to the column was sourced from a 25 L Nalgene carboy of de-ionized water (DIW). Flow rate was controlled using a micro-peristaltic pump, striving to maintain a constant flow rate of ~0.2 mL $min^{-1}$. However, the pump rate was increased at day 348 to 0.5 mL $min^{-1}$ so that the frequency of sample collection could be increased. The inflow water was flushed with nitrogen gas ($N_{2(g)}$) to remove dissolved oxygen (DO) from the porewater. Twenty-nine water sampling ports were located at 0.10 m intervals along the length of the column. Each port was equipped with 0.10 m long 1/8" PTFE tubing, which had been perforated along a 0.04 m section and filled with glass wool to act as a non-reactive filter. The perforated ends of the tubes were set inside the column while the outer ends were connected to one-way Luer lock valves on the outside of the column. Tubing was fitted to the column with bored-through stainless steel Swagelok 1/8" tube fittings with a 1/8" male NPT thread.

A 0.6 m section of the column located between 1.00 m and 1.60 m from the input end was designed to heat the water and sediments using cartridge heaters positioned at 0.1 m intervals and staggered radially. The column was also designed with a cooled section located between 1.90 m and 2.40 m from the input end, which consisted of stainless-steel cooling lines that ran inside the column to circulate cold water. Cooling water did not come in contact with column sediment or porewater. Fifteen temperature sensors,

including twelve thermistors and three Resistance Temperature Detectors (RTDs), were located along the entire length of the column to provide a temperature profile. Thermistors and RTD's were located at 0.10 m intervals in the heated section, at 0.20 m spacing from both ends of the heated section, and at 0.30 m intervals in all other sections of the column. A Campbell Scientific CR 1000 data logger was used to measure and control temperature.

A horizontal column alignment was used to minimize water density effects during heating. The end of the column outflow tubing was positioned 0.50 m higher than the column input water to achieve positive hydraulic pressure within the column. The column itself was housed in an anaerobic chamber. This was constructed using 0.5" thick clear acrylic panels welded together with a removable lid. The interface between the lid and the chamber walls was clamped together and sealed with a combination of a ¼" butyl rubber gasket and silicone caulking to ensure a gas tight fit along the perimeter edge. The input and output water and gas tubing were connected to the chamber using bored-through Swagelok threaded fittings sealed with PTFE tape. Holes that were drilled to house electrical wiring were sealed using silicon caulking.

To reduce the amount of DO entering the column a diaphragm pump under vacuum pressure was connected to the inflow tubing. The input water was regularly purged with nitrogen gas one to two times a week with a microporous gas bubbler for four to five hours. Prior to purging, the carboy was sealed using a PTFE lined cap with a fitted $N_{2(g)}$-filled Mylar® balloon and a connection to the output gas line to reduce the interaction of the input water with atmospheric oxygen. While the input water was purged one to two

times a week, the anaerobic chamber was constantly being purged as it was always connected to the $N_{2(g)}$ gas cylinder. Oxygen gas ($O_{2(g)}$) within the anaerobic chamber was monitored using an Apogee Instruments Inc. SO-210 fast response thermistor reference oxygen sensor.

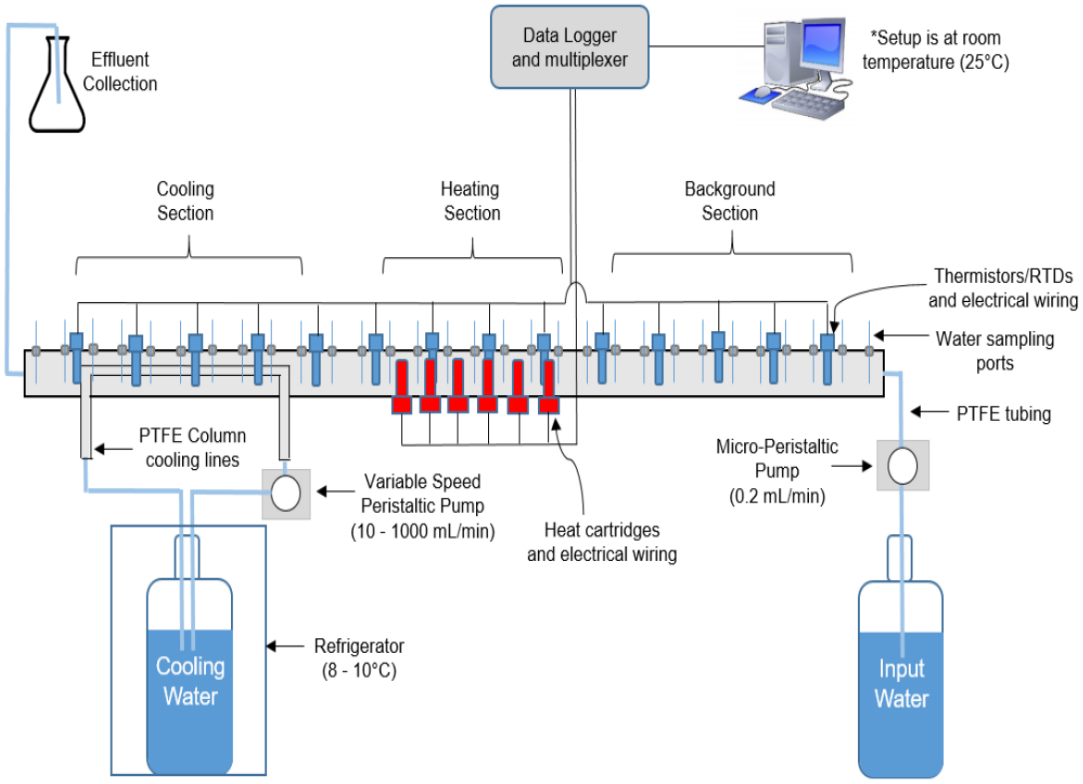


*Figure 3.1 Schematic design of the column set-up used throughout the duration of the experiment (Craig, 2017).*

## 3.2 Sampling Regime

Prior to the current study, involving the aquifer sediments collected from the Athabasca Oil Sands (In-Situ) area, experiments were conducted by Craig (2017) which involved the construction of the column, followed by characterization of chemical and physical properties of the column. This was achieved by filling the column with quartz sand mixed

with pyrite and included analyses of initial geochemical reactions within the column. The current study, conducted using the aquifer sediment, began in May 2017 by first thoroughly cleaning the inside of the column from previous experiments and then refilling it with the aquifer sediments; DIW was then pumped through the column and both the chamber and input water continued to be purged to minimize oxygen gas in the column (Craig, 2017).

Water samples were collected on a weekly basis during both the unheated and heated weeks, at 0.3 m intervals along the length of the column. Samples were collected at a frequency of one hour apart to allow enough time for replacement of the volume of water that was extracted. Due to the low volume of sample, analytical procedures were alternated throughout the sampling period and duplicate samples were not collected. Therefore, error bars are not presented on the plots within this text. During week one, samples were analyzed for DO, pH, and redox species including, sulphate ($SO_4^{2-}$) and sulphide ($S^{2-}$). During week two, samples were analyzed for the same parameters except for sulphide, which was replaced with analysis for ferrous iron ($Fe^{2+}$). During week 3, samples were collected for analysis of total elemental concentrations using both inductively coupled plasma optical emission spectrometry and inductively coupled plasma mass spectrometry (ICP-OES/MS). During the unheated study, pH, DO and sulphate were measured during the first three sampling weeks ( U5, U12, and U19), sulphide was measured during the first and third sampling weeks (U5 and U19), ferrous iron was measured during the second sampling week (U12), and ICP samples were collected during the last sampling week (U26).

The sampling regime was repeated throughout the experiment until day 352, when samples were collected 3 days/week instead of weekly; analysis then included pH, DO, and alkalinity one day, followed by pH, DO, sulphate, and sulphide, the next day, and pH, DO, sulphate, and ferrous iron on the final day each week. Other parameters were measured sporadically, including alkalinity, conductivity (Ec), and oxidation-reduction potential (ORP). Alkalinity was measured bi-weekly from weeks one to nine and again at weeks 41, 53, and 55. Conductivity and ORP measurements were taken at weeks 41, 53, and 55 and measured ORP values were used to calculate Eh.

Sample collection was performed by first purging 2 mL from the sample port to allow for a representative sample to be acquired. Afterwards, two 5 mL aliquots were collected from the port. All aqueous samples were filtered using a 0.45 μm polyethersulfone (hydrophilic) membrane filter. The first 5 mL aliquots were used for pH measurements and analysis of sulphate. The second 5 mL aliquot was used for DO measurements and analysis of either sulphide, or ferrous iron. Because both DO and pH measurements are relatively sensitive to time after sample collection, these readings were completed immediately before proceeding to redox species analysis. Samples collected from within the heated section of the column were left to sit for 1-2 minutes so that they would cool, and all samples were analysed at roughly the same temperature (~25 °C). Water samples collected for ICP-OES submission were collected as full 10 mL aliquots and acidified to a pH of 2 using $HNO_3$, then stored in sealed tubes in a refrigerator at ~4 °C. When alkalinity measurements were taken, the first 5 mL aliquot was used for DO while the next was used for pH, alkalinity, conductivity, and ORP. A series of blank samples were also submitted to test the potential for contamination from the sample syringe, filter,

sample tube, the tube cap, as well as the DIW. All equipment was cleaned using 2% $HNO_3$. Effluent water was collected from the output tubing during the experiment to monitor flow rate.

The pH was analyzed at the time of sampling using a double-junction Cole Parmer ATC pH/temperature probe connected to an Oakton Ion 700 meter. DO was measured with an Oakton DO 6+ meter and DO probe. Sulphate, sulphide, and ferrous iron concentrations were measured using the Hach USEPA SulfaVer 4, methylene blue and 1,10-phenanthroline methods, respectively. Total alkalinity was measured using the Hach TNT plus 870 Colorimetric method. Conductivity and ORP measurements were measured using a VWR symphony H30PCO meter and 89231-656 probe.

## 3.3 Sediment Characterization

The sediments used in this experiment were provided by the Alberta Geological Survey from borehole WR99-1 (Coordinates: 55.7143794 °N 112.1879148 °W,) located within the Athabasca Oil Sands (In-Situ) region (Figure 3.2; Craig, 2017;Parks & Andriashek, 2002). The core material was collected between depth intervals 122 to 134 m and 208 to 213 m, from the Empress Formation Unit 3. Before originally being poured into the column, the aquifer material was mixed thoroughly using equal volumes of sediments from both depth intervals (Craig, 2017). The sediment was characterized by Craig (2017) prior to the heated study; the sediment was then characterized again, as a part of the current study, at the end of the heated column experiment.

A combination of X-ray diffraction (XRD), X-ray fluorescence (XRF), scanning electron

micro probe-energy-dispersive X-ray spectroscopy (SEM-EDX or SEM), and aqua regia digestion, followed by analysis via ICP-OES, was used to characterize the bulk mineralogy and total elemental composition of the sediments, respectively, before being placed in the column (prior to the heated study; Craig, 2017). Bulk XRD was performed in two separate scans. The parameters used in the first scan were used to identify major silicate and non-silicate minerals, while the slower step-width of the second scan was used to identify less abundant minerals which were emulated from Javed et al. (2014) to allow for comparisons to be made. XRF and SEM were performed on the sediments to identify quantitative elemental trends.

After completion of the heated experiment, XRD was again used to characterize the bulk minerology, coupled with the use of electron micro probe analysis (EMPA) and an energy-dispersive detector (EDS), to gain an understanding of the changes in elemental composition within the sediment due to the high temperature range implemented within the column over the year-long study. These analyses were also conducted to locate sources and sinks of arsenic within the column. EMPA was used in three trials. In the first trial EMPA was used to analyze silicates, oxides, and clays. Energy-dispersive X-ray spectroscopy (EDS) was used to characterize any grains that were seen that were not a part of the bulk minerology. Any grains that did not fall under the silicates/oxides/clays category were analyzed as either sulphides or phosphates in two separate trials, depending on indication via EDS on which types of grains they may be. Eleven thin sections were analyzed, consisting of sediment samples from 0.02-2.9 m along the length of the column. Three of these samples were from the heated section and one was from the cooled section (Figure 3.3). They were chosen based on amount of sample material

available.

Geochemical modelling of the column experiment results was carried out using PHREEQC Version 3 (Parkhurst & Appelo, 2013). This was coupled with the MINTEQ database due to its suitability for systems where temperatures are between 25-100 °C (Allison, Brown, & Novo-gradac, 1991) and demonstrated accuracy for calculating quartz solubility at high temperatures (Appelo & Postma, 2005). Modelling was performed to determine the saturation indices (SI) of particular minerals at each sampling port along the column and at various times throughout the study to determine the nature of water-rock interactions that occurred within the column. These minerals included quartz, feldspar, muscovite, calcite, ferrihydrite, gibbsite, hydroxyapatite, strengite, vivianite, gypsum, and $O_{2(g)}$. The input for the model consisted of the aqueous geochemical data that was collected throughout the year. For sampling days where aqueous concentrations of alkalinity, silica, and sulphide were not available, averages of the data that was available was used.

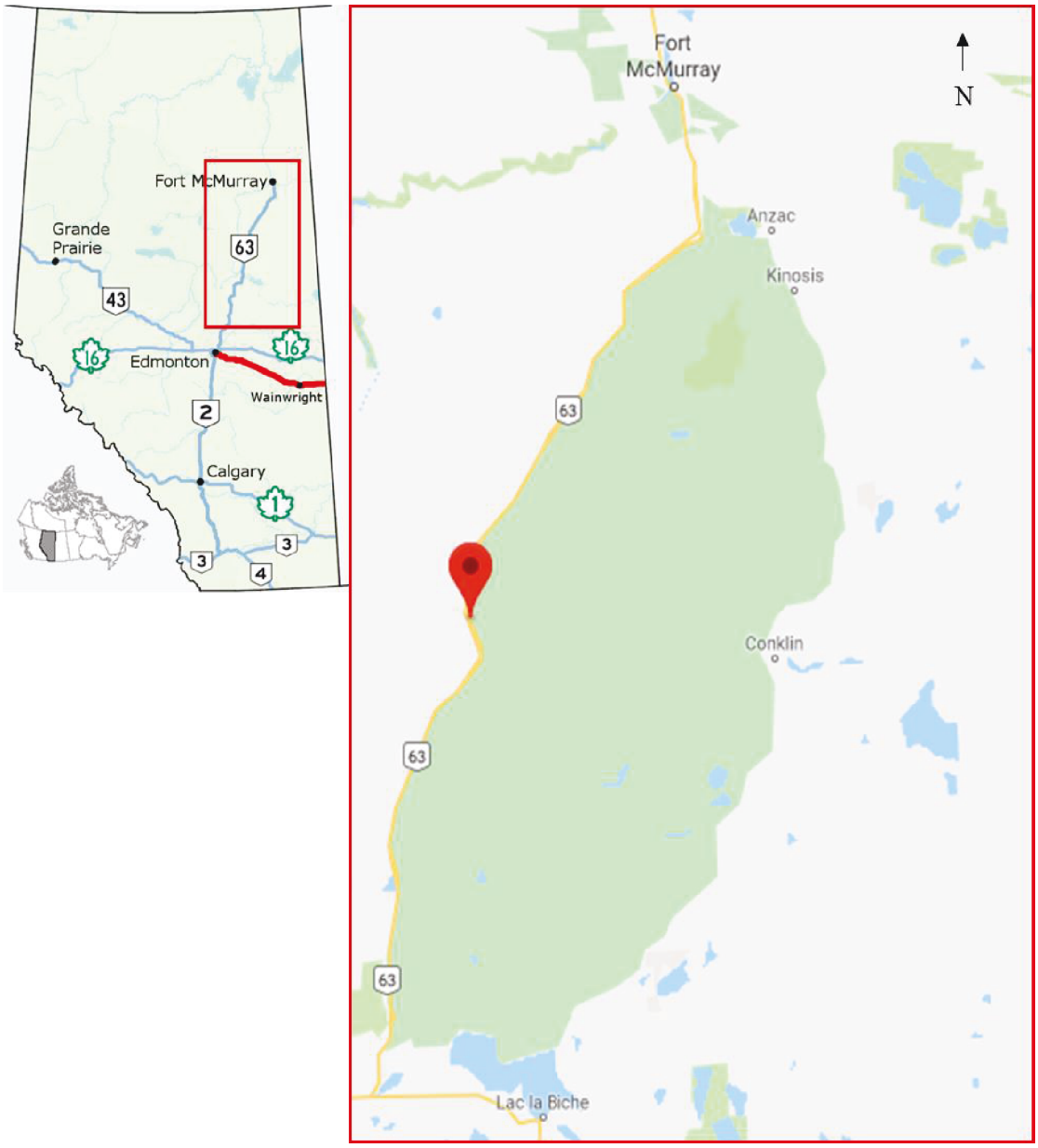


*Figure 3.2 Location of collected sediment, from borehole WR99-1, relative to Fort McMurray and Cold Lake (Google Maps, 2019) within Alberta, Canada (Acefitt, 2017).*

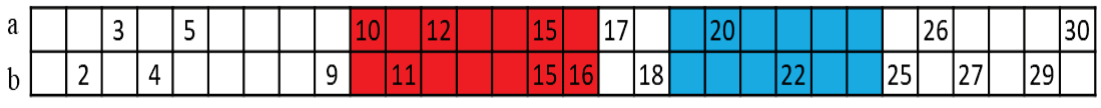


*Figure 3.3 Column schematic depicting locations where sediment was collected and used to make the thin sections analyzed using XRD (a) and EMPA (b). The heated section of the column is highlighted in red whereas the cooled section is highlighted in blue. Each number represents the total length along the column in cm (i.e. Section 2 is 20 cm from the input whereas section 30 is 300 cm from the input).*

# 4.0 Results

## 4.1 Conditions Within the Column

### 4.1.1 Physical Conditions

During the unheated study (U5-U26), average temperature within the column remained slightly above room temperature at an average of 25.3 ± 3.0 °C (Figure 1.1). During the heated study (days 5-375), temperature varied within the column and during each sampling period. Temperatures recorded at 0.3 m along the length of the column generally ranged from 25.5-32.0 °C. By 0.6 m, temperature had increased slightly to between 25.0-36.5 °C, then quickly rose to approximately 86.0 °C by 1.6 m (in the heated section). From 1.9-2.4 m (in the cooled section), temperatures decreased sharply to between 18.0 and 25.5 °C. From days 352-375 temperature fell only as low as ~25.0 °C within the cooled section, as the efficiency of the cooling loop appears to have decreased. Within the last 0.6 m of the column the temperature rose slightly to between 25.5-28.5 °C. Temperatures varied the least during the unheated study, as it varied by no more than ± 0.5 ºC during each day of sampling. During the heated study, temperatures varied by as much as 11.5 ºC between the sampling days.

Despite efforts to maintain constant flow rate, the flow rate did vary during the experiment (Figure 4.2); in general, it ranged from 0.10-0.30 mL $min^{-1}$ during the entire experiment. Flow rate remained relatively constant in the first 60 days of the experiment. During this period, flow rate was at an average of 0.21 ± 0.01 mL $min^{-1}$. By day 103, flow rate had decreased and remained relatively constant until day 187. During this

period flow rate was at an average of 0.14 ± 0.01 mL $min^{-1}$. Beyond that day, flow rate was much more varied, perhaps partially due to the effects of sampling. By day 232 flow rate had decreased to as low as 0.01 mL $min^{-1}$. A manual pump speed adjustment was conducted on that day to increase the flow rate, resulting in it generally increasing over time, and by day 284 it was 0.16 mL $min^{-1}$. Another manual pump speed adjustment was conducted near the end of the experiment to increase flow rate, resulting in flow rate from days 348-372 ranging from 0.26-0.70 mL $min^{-1}$.

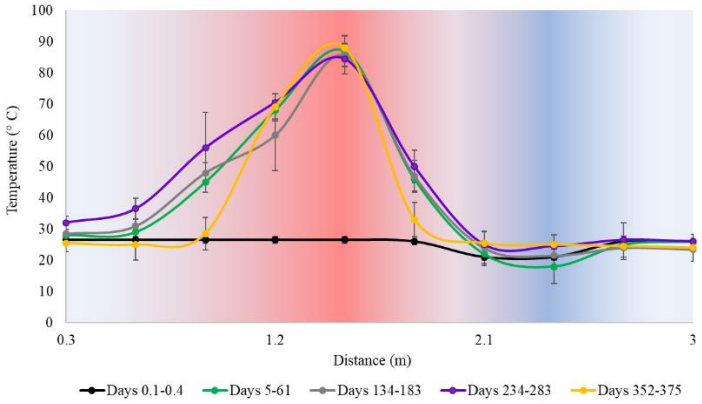


*Figure 4.1 Average temperatures along the length of the column throughout various periods during the experiment. This plot, and all others like it, were underlain by a colour gradient representing heated (red), cooled (blue) and neutral (white) parts of the column.*

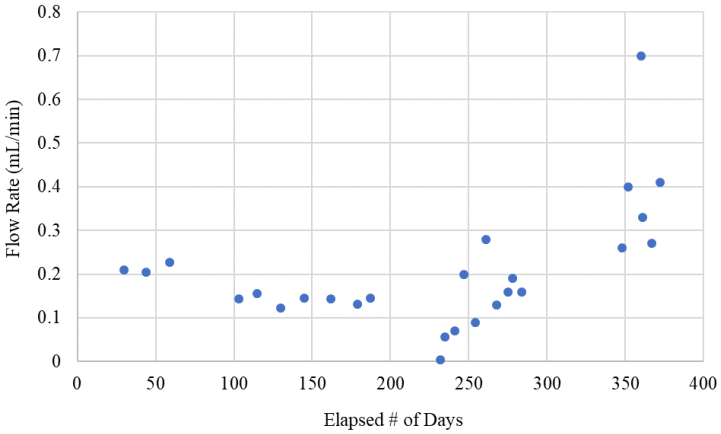


*Figure 4.2 Flow rate within the column throughout the experiment.*

### 4.1.2 Porewater Geochemistry

During the unheated study, pH was circumneutral and relatively consistent throughout the entire column and sample period, ranging from 6.7-7.3 (Figure 4.3a). During the first 2 sampling days of the unheated study it ranged from 6.7-7.0, while it was slightly higher during the last day of the sampling period, ranging from 7.1-7.3. During the heated study, pH was acidic to basic, as it varied within the different sections of the column. Within the first 1.2 m of the column pH ranged from 6.0-8.0 with the exception of days 169 and 234, where the pH ranged from 5.5-6.5. The pH recorded at 1.5 m was slightly higher and ranged from 7.0-9.0, with the exception of day 234 where the pH was as low as 5.5. From 1.8-2.1 m along the length of the column pH had decreased and ranged from 6.5-8.0, with the exception of day 234 where the pH was as low as 5.5-6.0. Within the last 0.6 m of the column the pH generally ranged from 7.0-8.0, with the exception of days 169, 234, 352, and 366 where the pH ranged from 5.0-6.5 and at day 362 where the pH was as high as 9. The greatest pH range was within the beginning of the column, while pH was more consistent at the end of the column.

During the heated study, alkalinity generally increased from the beginning to the end of the column, from an initial range of 8.3-60.0 mg $L^{-1}$ $CaCO_3$ to a final range of 20-110 $CaCO_3$ (Figure 4.3b). From days 19-47, alkalinity appeared to follow a steady trend of increasing from the beginning to the end of the column, while from days 283-366 alkalinity was more varied, as it was found to oscillate as well as increase throughout the column. Peaks of alkalinity concentration were at 0.6, 1.5, and 2.7 m along the length of the column, whereas troughs were observed at 0.9, 1.2, 1.8, and 2.4 m along the length of

the column. Sampling from days 19-47 included less sampling points so it is possible that oscillations were not detected during those days. Furthermore, there was a greater range of alkalinity at the end of the column than at the beginning of the column. In addition, alkalinity from days 19-47 decreased overall. At day 19, alkalinity within the column ranged from 13.4-78.6 mg $L^{-1}$ $CaCO_3$. By day 47 it ranged from 8.25-61.0 mg $L^{-1}$ $CaCO_3$. By day 283 it had increased and ranged from 60.0-110 mg $L^{-1}$ $CaCO_3$ but, by day 366 concentrations had decreased again and ranged from 12.5-20 mg $L^{-1}$ $CaCO_3$.

During the heated study, Eh was found to vary between the different sections of the column (Figure 4.3c) Within the first meter of the column, Eh ranged from 0.30-0.61 V. From 1.2-1.5 m Eh decreased, to a minimum of 0.20-0.30 V. From 1.8-2.1 m Eh had increased to a range of 0.30-0.45 V. Within the last 0.6 m of the column Eh remained at 0.30-0.40 V. The greatest variability exhibited by Eh was within the first meter of the column, whereas the least amount of variability in Eh was observed at the end of the column. Furthermore, Eh was more consistent throughout the column at day 283, at an average Eh of 0.29 ± 0.03 V. During days 352 and 366 it was more varied, as peaks at 0.9 and 2.1 m along the length of the column ranged from 0.40-0.61 V and 0.42-0.44 V, respectively, and the trough at 1.5 m was as low as 0.20-0.26 V. The phase diagrams for iron and sulphate overlain by the Eh and pH throughout the column suggest that despite the changing conditions within the heated section of the column, the stability of these phases would not change significantly (Figure 4.6a-f). The stability of arsenic, however, may have changed in response to pH, according to its phase diagram.

During the unheated study DO ranged from 2.1-3.7 mg $L^{-1}$ (Figure 4.3d). During the first

and last days during this sampling period, DO varied throughout the column, generally decreasing from 3.3-3.5 at 0.9 m along the length of the column, to 2.1-3.1 mg $L^{-1}$ at 1.5 m. During the second sample day it generally increased from the beginning to the end of the column, from an initial concentration of 3.5 mg $L^{-1}$ at 0.3 m along the length of the column to a final concentration of 3.2 mg $L^{-1}$ at 3.0 m along the length of the column. During the heated study, DO varied within the different sections of the column. Overall it ranged between 1.0-4.5 mg $L^{-1}$. Within the first meter of the column, DO ranged from 1.5-4.5 mg $L^{-1}$. From 1.2-1.8 m DO decreased slightly to a minimum of 1.5-3.5 mg $L^{-1}$, with the exception of days 61, 183, 283, and 362, where DO increased relative to values from the other ports along the column. From 2.1-3.0 m DO slightly increased to values reflecting those from the first meter of the column, at a range of 1.5-4.5 mg $L^{-1}$, with the exception of days 362 and 368, where DO decreased and ranged from 1-1.5 mg $L^{-1}$. DO exhibited the greatest variability in the beginning and end of the column; between 0.3-0.9 m and 2.1-0.3 m. The least amount of variability was observed within the section from 1.2-1.8 m along the length of the column.

During the heated study, conductivity was found to vary greatly (Figure 4.3e). During day 283, conductivity increased from 0.3-0.9 m along the length of the column, from 109 us $cm^{-1}$ at 0.3 m to 173 us $cm^{-1}$ at 0.9 m. It then decreased, to a minimum of 104 us $cm^{-1}$ at 1.8 m. By 2.1 m along the length of the column it had increased again and was at 208 us $cm^{-1}$. It then remained relatively consistent until the end of the column at 3.0 m. At day 362 conductivity decreased from 136 us $cm^{-1}$ at 0.3 m along the length of the column, to 84 us $cm^{-1}$ at 1.2 m. It then remained relatively consistent until 2.4 m, where conductivity had again decreased and was 51 us $cm^{-1}$. By 3.0 m it had decreased only slightly and was

48 us $cm^{-1}$. At day 366, conductivity was 257 us $cm^{-1}$ at 0.3 m along the length of the column. By 0.6 m it had decreased to 59 us $cm^{-1}$ but by 0.9 m increased and was 202 us $cm^{-1}$. By 1.2 m along the length of the column it was 67 us $cm^{-1}$, and it remained relatively consistent until 2.1 m, where it was 76 us $cm^{-1}$. It then increased and by 3.0 m at the end of the column it was 114 us $cm^{-1}$.

During the first day of sampling during the unheated study, sulphate increased from 80 mg $L^{-1}$ at 0.3 m along the length of the column, to 855 mg $L^{-1}$ at 1.2 m along the length of the column, then generally decreased, and by 3.0 m was 470 mg $L^{-1}$ (Figure 4.3f). During the second and third days of the unheated study, sulphate generally increased from the beginning to the end of the column from an initial range of 72-140 mg $L^{-1}$ to a final range of 840-846 mg $L^{-1}$. During the heated study from days 5-61, sulphate followed a similar trend of increasing from the beginning to the end of the column as was the case in the unheated study. However, it decreased overall each week. At day 5, sulphate ranged from 32-630 mg $L^{-1}$ but, by day 61 ranged from 2-14 mg $L^{-1}$. From days 134-183, concentrations generally remained low (2-10 mg $L^{-1}$) throughout the column, except at 1.5 m along the length of the column, where concentrations ranged from 140-240 mg $L^{-1}$. During days 234-369, sulphate was consistently below 100 mg $L^{-1}$ and did not vary much between different sections of the column with the exception of days 208, 353, and 366. At day 208, sulphate varied greatly and oscillated throughout the column at a concentration of 211 ± 105 mg $L^{-1}$. At day 353, another spike at 1.5 m was observed, at a concentration of 368 mg $L^{-1}$. At day 366, sulphate was as high as 214 mg $L^{-1}$ at 0.6 m along the length of the column.

During the first day of the unheated study, sulphide was consistent from 0.3-0.9 m at 0.030-0.032 mg $L^{-1}$, but at 1.2 m it began to increase and by 1.5 m it was at 0.010 mg $L^{-1}$. It did not then change significantly until 2.7 m, where it dropped back to 0.032 mg $L^{-1}$, then increased again to 0.01 mg $L^{-1}$ (Figure 4.3g). By the next sample day, it was relatively consistent throughout the column at 0.027 ± 0.002 mg $L^{-1}$. During the heated study, sulphide varied between sections of the column. From days 5-169, sulphide was relatively consistent throughout the column, as was the case in the unheated study. However, concentrations decreased overall during those days, from an initial range of 0.020-0.024 mg $L^{-1}$ at day 5 to 0.008-0.010 mg $L^{-1}$ by day 169, with the exception of day 61 where concentrations increased from the beginning to the end of the column, from an initial concentration of 0.036 mg $L^{-1}$ to a final concentration of 0.062 mg $L^{-1}$. During days 234 and 352, sulphide was at values reflecting concentrations seen during the unheated study, with the exception of sulphide at 1.8 m along the length of the column, where concentrations were as high as 0.024-0.070 mg $L^{-1}$. From days 362-366 concentrations were below the detection limit (0.005 mg $L^{-1}$) throughout the column, with the exception of sulphide at 0.9 and 2.1 m along the length of the column, where concentrations were as high as 0.024 and 0.040 mg $L^{-1}$, respectively. Day 269 exhibited sulphide concentrations, which were the most varied, oscillating around a concentration of 0.045 ± 0.040 mg $L^{-1}$.

During the unheated study, ferrous iron increased from the beginning to the end of the column, from an initial concentration of 0.95 mg $L^{-1}$ to a final concentration of 2.25 mg $L^{-1}$ (Figure 4.3h). During the heated study, ferrous iron varied within the different sections of the column. At day 19, ferrous iron followed a similar trend of increasing from the beginning to end of the column, as was the case in the unheated study. At 0.3 m

along the length of the column it was at a concentration of 0.02 mg $L^{-1}$ and by 3.0 m was at 0.20 mg $L^{-1}$. At day 47, it was relatively consistent throughout the column, at 0.30 ± 0.02 mg $L^{-1}$. By day 148 ferrous iron decreased overall to a point where it was almost entirely below the detection limit (DL = 0.02 mg $L^{-1}$) throughout the entire column. From days 183-362, it had become elevated in the last half of the column, from 1.5-3.0 m. Here, concentrations ranged from 0.03-0.10 mg $L^{-1}$, with the exception of day 352 at 1.5 m along the length of the column, where it was as high as 0.15 mg $L^{-1}$. At day 366, ferrous iron concentrations were elevated in the first half of the column, from 0.3-1.5 m. Here, it ranged from 0.05-0.10 mg $L^{-1}$. The greatest variability of ferrous iron concentrations was observed within the last half of the column, from 1.5-3.0 m.

During the unheated study, phosphorous was below the detection limit (DL = 0.03 mg $L^{-1}$) from 0.3-2.1 m along the length of the column (Figure 4.4a). From 2.4-3.0 m along the length of the column phosphorous averaged at a concentration of 0.06 ± 0.01 mg $L^{-1}$. During the heated study, phosphorous varied within the different sections of the column. From 0.3-0.9 m along the length of the column it increased from an initial range of below the detection limit -0.07 mg $L^{-1}$ to a final range of 0.06-0.09 mg $L^{-1}$. By 1.5 m along the length of the column phosphorous had decreased and was 0.06 mg $L^{-1}$. Concentrations increased to a maximum range of 0.07-0.10 mg $L^{-1}$ by 2.4 m along the length of the column. At 2.4 m and 3.0 m concentrations had decreased slightly, at ranges of 0.05-0.08 mg $L^{-1}$ and 0.06-0.09 mg $L^{-1}$, respectively. In general, phosphorous concentrations increased throughout the study, from an initial range of below the detection limit to 0.06 mg $L^{-1}$ during the unheated study, to a final range of 0.07-0.09 mg/L by day 54 of the heated study, which is the last day phosphorous measurements are available..

During the unheated study, silica increased from the beginning to the end of the column, from an initial concentration of 6.19 mg $L^{-1}$ to a final concentration of 14.51 mg $L^{-1}$ (Figure 4.4b). During the heated study, silica concentrations increased in the heated section of the column and decreased slightly in the cooling section toward the end of the column. At 0.3 m along the length of the column, silica ranged from 3.74-4.90 mg $L^{-1}$. From 0.6-0.9 m silica sharply increased. Concentrations at 0.9 m along the length of the column ranged from 14.20-17.98 mg $L^{-1}$. Concentrations remained relatively consistent until 2.4 m along the length of the column. Here concentrations decreased consistently toward the end of the column, from an initial range of 14.98-16.75 mg $L^{-1}$ to a final range of 11.38-13.57 mg $L^{-1}$.

During the unheated study, Ca generally increased from the beginning to the end of the column, from an initial concentration of 78 mg $L^{-1}$ at 0.3 m along the length of the column to a final concentration of 573 mg $L^{-1}$ at 3.0 m along the length of the column (Figure 4.4c). During the heated study, calcium was found to have increased from the beginning of the column to the end of the column, as was the case in the unheated study, with the exception of a plateau within the heated section of the column. From 0.3-0.9 m along the length of the column calcium increased from a range of 3-24 mg $L^{-1}$ to a range of 3.8-62 mg $L^{-1}$. From 1.2-1.8 m along the length of the column calcium remained relatively consistent, as it ranged from 5-65 mg $L^{-1}$ at 1.2 m and 5-70 mg $L^{-1}$ at 1.8 m. From 2.1-3.0 m calcium increased from a range of 6-93 mg $L^{-1}$ to a range of 8-241 mg $L^{-1}$. During the experiment concentrations decreased each week, from an initial range of 78-573 mg $L^{-1}$ during the unheated study to a final range of 3-8 mg $L^{-1}$ by the end of the heated study.

During the unheated study, sodium generally increased from the beginning to the end of the column, from an initial concentration of 9 mg $L^{-1}$ at 0.3 m along the length of the column to a final concentration of 466 mg $L^{-1}$ at 3.0 m along the length of the column (Figure 4.4d). During the heated study, the same trend was observed, with the exception of a plateau within the heated section. From 0.3-0.9 m along the length of the column sodium increased from a range of 0.59-4.65 mg $L^{-1}$ to a range of 1.59-11.74 mg $L^{-1}$. From 1.2- 2.1 m along the length of the column sodium was relatively consistent, as it ranged from a range of 2.87-12.62 mg $L^{-1}$ to a range of 2.42-15.50 mg $L^{-1}$. From 2.4-3.0 m along the length of the column, sodium increased from a range of 2.45-20.15 mg $L^{-1}$ to a final range of 3.95-179.33 mg $L^{-1}$. Overall, concentrations decreased each week, from an initial range of 9-466 mg $L^{-1}$ during the unheated study to a final range of 0.73-4.74 mg $L^{-1}$ by the end of the heated study.

During the unheated study, potassium increased from the beginning to the end of the column, from an initial concentration of 2.9 mg $L^{-1}$ to a final concentration of 29.9 mg $L^{-1}$ (Figure 4.4e). During the heated study, the same trend was observed, with the exception of a plateau from 1.2-2.1 m along the length of the column. From 0.3-0.9 m along the length of the column potassium increased from a range of 0.3-1.3 mg $L^{-1}$ to a final range of 0.5-6.4 mg $L^{-1}$. From 1.2-2.1 m along the length of the column it remained relatively constant, as at 1.2 m potassium ranged from 0.8-6.9 mg $L^{-1}$ and at 2.1 ranged from 0.9-7.5 mg $L^{-1}$. From 2.4-3.0 m along the length of the column potassium increased, from a range of 0.9-7.2 mg $L^{-1}$ to a final range of 1.2-10.5 mg $L^{-1}$. Furthermore, potassium concentrations decreased each week throughout the study, from an initial range of 2.9-29.9 mg $L^{-1}$ during the unheated study, to a final range of 0.3-1.2 mg $L^{-1}$ by the final day

of the heated study.

During the unheated study, magnesium increased from the beginning to the end of the column, from an initial concentration of 7.9 mg $L^{-1}$ to a final concentration of 110.0 mg $L^{-1}$ (Figure 4.4f). During the heated study, the same trend was observed, with the exception of a plateau from 0.9-1.8 m along the length of the column. Magnesium was found to increase from 0.3-0.9 m along the length of the column, from a range of 0.20-2.13 mg $L^{-1}$ to a range of 0.21-4.38 mg $L^{-1}$. Magnesium then remained relatively constant until 2.1 m. Generally, magnesium increased from 2.1-3.0 m along the length of the column, from a range of 0.24-7.31 mg $L^{-1}$ to a final range of 0.83-29.18 mg $L^{-1}$. Overall, concentrations throughout the study decreased each week, from 7.87-110.01 mg $L^{-1}$ during the unheated study to 0.20-0.83 mg $L^{-1}$ by the final day of the study.

During the unheated study, arsenic concentrations were found to be relatively constant at $0.0017 \pm 0.0002$ mg $L^{-1}$ from 0.3 to 1.8 m along the length of the column, then increased to a final concentration of 0.0064 mg $L^{-1}$ at the end of the column (Figure 4.5a). During the heated study, arsenic concentrations increased in the heated section of the column and decreased in the cooling section toward the end of the column. At 0.3 m along the length of the column, arsenic ranged from 0.002-0.004 mg $L^{-1}$. From 0.6-1.2 m arsenic generally increased, from an initial range of 0.0026-0.0067 mg $L^{-1}$ at 0.6 m to a final range of 0.0048-0.0088 mg $L^{-1}$ at 1.2 m. Concentrations remained relatively constant throughout the heated section within the next meter, as at 1.2 m along the length of the column it ranged from 0.0048-0.011 mg $L^{-1}$ and at 1.8 m ranged from 0.0053-0.0100 mg $L^{-1}$. Beyond 2.1 m, concentrations decreased consistently toward the end of the column and

by 3.0 m it ranged from 0.0027-0.0037 mg $L^{-1}$; reflective of concentrations observed at the beginning of the column.

During the unheated study, aluminum remained consistently below the detection limit (DL = 0.010 mg $L^{-1}$) throughout the column (Figure 4.5b). During the heated study, aluminum increased sharply within the heated section of the column and decreased sharply within the cooled section of the column, so that concentrations at the end of the column mirrored those at the beginning. From 0.3-0.9 m along the length of the column concentrations remained relatively consistent and ranged from 0.013-0.017 mg $L^{-1}$. At 1.2 m along the length of the column concentrations had increased slightly and ranged from 0.011-0.027 mg $L^{-1}$. By 1.5 m along the length of the column aluminum had increased greatly and ranged from 0.042-0.367 mg $L^{-1}$. This was followed by a decrease of similar magnitude, and by 1.8 m concentrations ranged from less than the detection limit to 0.050 mg $L^{-1}$. From 2.1-3.0 m along the length of the column concentrations continued to decrease until they had reached below the detection limit, with the exception of day 359, where there was a spike in aluminum at 2.7 m along the length of the column, to 0.040 mg $L^{-1}$.

During the unheated study, titanium concentrations were below the detection limit (DL = 0.0025 mg $L^{-1}$) from 0.3-1.5 m along the length of the column (Figure 4.5c). From 1.8-3.0 m along the length of the column titanium increased from a concentration of 0.0026 mg $L^{-1}$ to a concentration of 0.0038 mg $L^{-1}$. During the heated study, titanium concentrations generally increased within the heated section of the column and decreased slightly within the cooled section of the column. At 0.3 m along the length of the column,

titanium ranged from 0.005-0.009 mg $L^{-1}$. From 0.6-1.8 m titanium generally increased; by 1.8 m it ranged from 0.0018-0.0048 mg $L^{-1}$. By 2.1 m along the length of the column concentrations had generally decreased and here they ranged from 0.0018-0.0036 mg $L^{-1}$. In general, titanium continued decreasing and by 3.0 m along the length of the column it ranged from 0.0013-0.0031 mg $L^{-1}$; values higher than concentrations observed at the beginning of the column.

During the unheated study, zinc remained relatively consistent throughout the column, at a concentration of 0.022 ± 0.008 mg $L^{-1}$ (Figure 4.5d). During the heated study, zinc concentrations varied within the different sections of the column. In general, concentrations increased from 0.3-1.5 m along the length of the column, from concentrations ranging from 0.004-0.053 mg $L^{-1}$ to concentrations ranging from 0.024-0.131 mg $L^{-1}$, with the exception of days 141 and 176 where there was a spike at 1.2 m where concentrations reached as high as 0.308 mg $L^{-1}$. By 2.1 m, concentrations had decreased to 0.005-0.173 mg $L^{-1}$ but, there was another spike at 2.4 m along the length of the column from days 141-227, where concentrations were as high as 0.19 mg $L^{-1}$. At 3.0 m along the length of the column concentrations had generally decreased to 0.004-0.050 mg $L^{-1}$, with the exception of days 176 and 255, which remained as high as 0.207 mg $L^{-1}$ and 0.143 mg $L^{-1}$, respectively.

During the unheated study, total iron remained consistently below the detection limit (DL1 = 0.025 mg $L^{-1}$) throughout the column (Figure 4.5e). During the heated study, total iron remained below the detection limit throughout the entire column during days 5-54, with the exception of spikes at 0.3 m, 0.6 m, and 3.0 m along the length of the column

during days 40, 26, and 12, respectively. Concentrations at these spikes ranged from 0.032-0.052 mg $L^{-1}$. During days 141-255 the detection limit was reduced (DL2 = 0.0002 mg $L^{-1}$). During those days, total iron concentrations from 0.3-1.5 m along the length of the column ranged from 0.0006-0.0151 mg $L^{-1}$. By 2.1 m along the length of the column concentrations had increased and ranged from 0.0046-0.0291 mg $L^{-1}$. By 2.4 m along the length of the column concentrations had decreased and from 2.4-3.0 m along the length of the column concentrations remained relatively consistent and ranged from 0.0004-0.0032 mg $L^{-1}$. Iron was likely oxidized within the entire system.

During the unheated study, copper increased from the beginning to the end of the column, from an initial concentration of 0.0020 mg/L to a final concentration of 0.0150 mg/L (Figure 4.5f). During the heated study, copper generally decreased within the heated section of the column and increased within the cooled section of the column, to final concentrations reflective of initial concentrations observed at the beginning of the column. At 0.3 m along the length of the column concentrations ranged from 0.0003-0.0022 mg $L^{-1}$. Concentrations were then found to decrease and by 0.9 m along the length of the column copper ranged from 0.0003-0.0008 mg $L^{-1}$. Concentrations did not change significantly until 2.1 m, with the exception of spikes observed during days 12 and 141, where concentrations were as high as 0.0020 mg $L^{-1}$ and 0.0036 mg $L^{-1}$, respectively. From 2.1-3.0 m along the length of the column concentrations steadily increased, to a final range of 0.0008-0.0024 mg $L^{-1}$.

During the unheated study, manganese concentrations increased from 0.21 mg $L^{-1}$ at 0.3 m to 0.30 mg $L^{-1}$ at 0.9 m (Figure 4.5g). There was a spike in concentration at 1.2 m

along the length of the column, where manganese was as high as 0.93 mg $L^{-1}$, followed by a decrease to 0.30 mg $L^{-1}$ at 2.4 m before increasing to a final concentration of 0.46 mg $L^{-1}$ at 3.0 m along the length of the column. During the heated study from days 5-54, manganese generally increased from the beginning to the end of the column, from an initial range of 0.107-0.262 mg $L^{-1}$ to a final range of 0.169-0.895 mg $L^{-1}$ but, decreased overall each week. By day 141, manganese concentrations were relatively consistent throughout the entire column, ranging from 0.012-0.057 mg $L^{-1}$, with the exception of a spike at 2.1 m, which ranged from 0.056-0.132 mg $L^{-1}$.

During the unheated study, nickel concentrations increased from 0.004 mg $L^{-1}$ at 0.3 m to a concentration of 0.006 mg $L^{-1}$ at 0.9 m (Figure 4.5h). Concentrations then increased sharply to 0.020 mg $L^{-1}$ by 1.5 m before decreasing to a concentration of 0.008 mg $L^{-1}$ at 1.8 m along the length of the column and slightly increased to a final concentration of 0.012 mg $L^{-1}$ at 3.0 m along the length of the column. During the heated study, nickel was relatively constant from 0.3-1.5 m along the length of the column, then increased towards the end of the column. At 0.3 m along the length of the column, nickel ranged from below the detection limit (DL = 0.001 mg $L^{-1}$) to 0.003 mg $L^{-1}$ and was the same at 1.5 m. Nickel generally increased from a range of below the detection limit to 0.007 mg $L^{-1}$ at 1.8 m, to a range of 0.001-0.011 mg $L^{-1}$, with the exception of day 12. During day 12, nickel dropped at 1.5 m along the length of the column to a concentration much lower than those seen that day; as low as 0.002 mg $L^{-1}$.

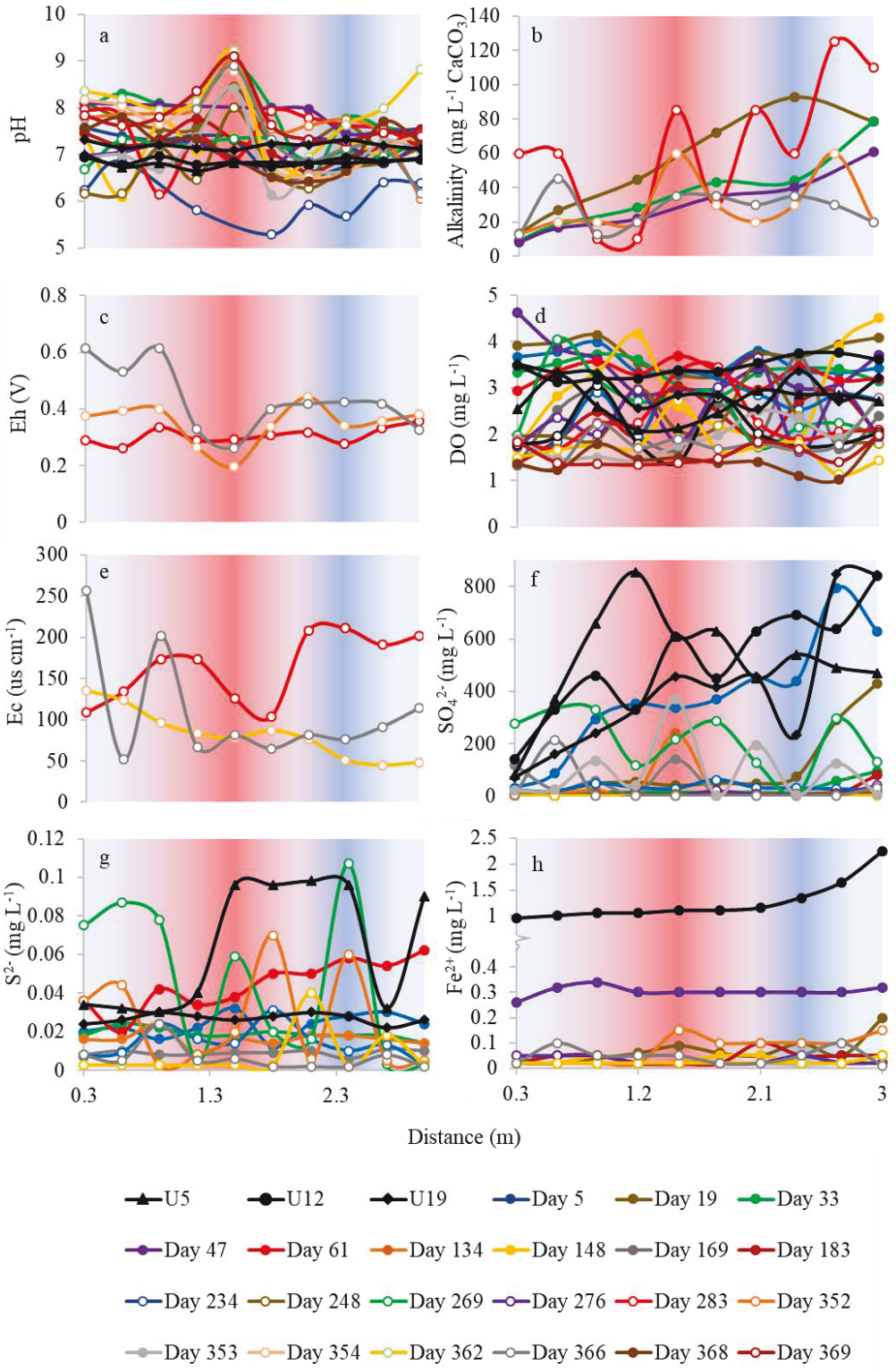


*Figure 4.3 pH (a), alkalinity (b), Eh (c), DO (d), conductivity (e), sulphate (f), sulphide (g), and ferrous iron (h) along the length of the column throughout the unheated and heated studies. Any samples that had concentrations <DL were plotted as the DL.*

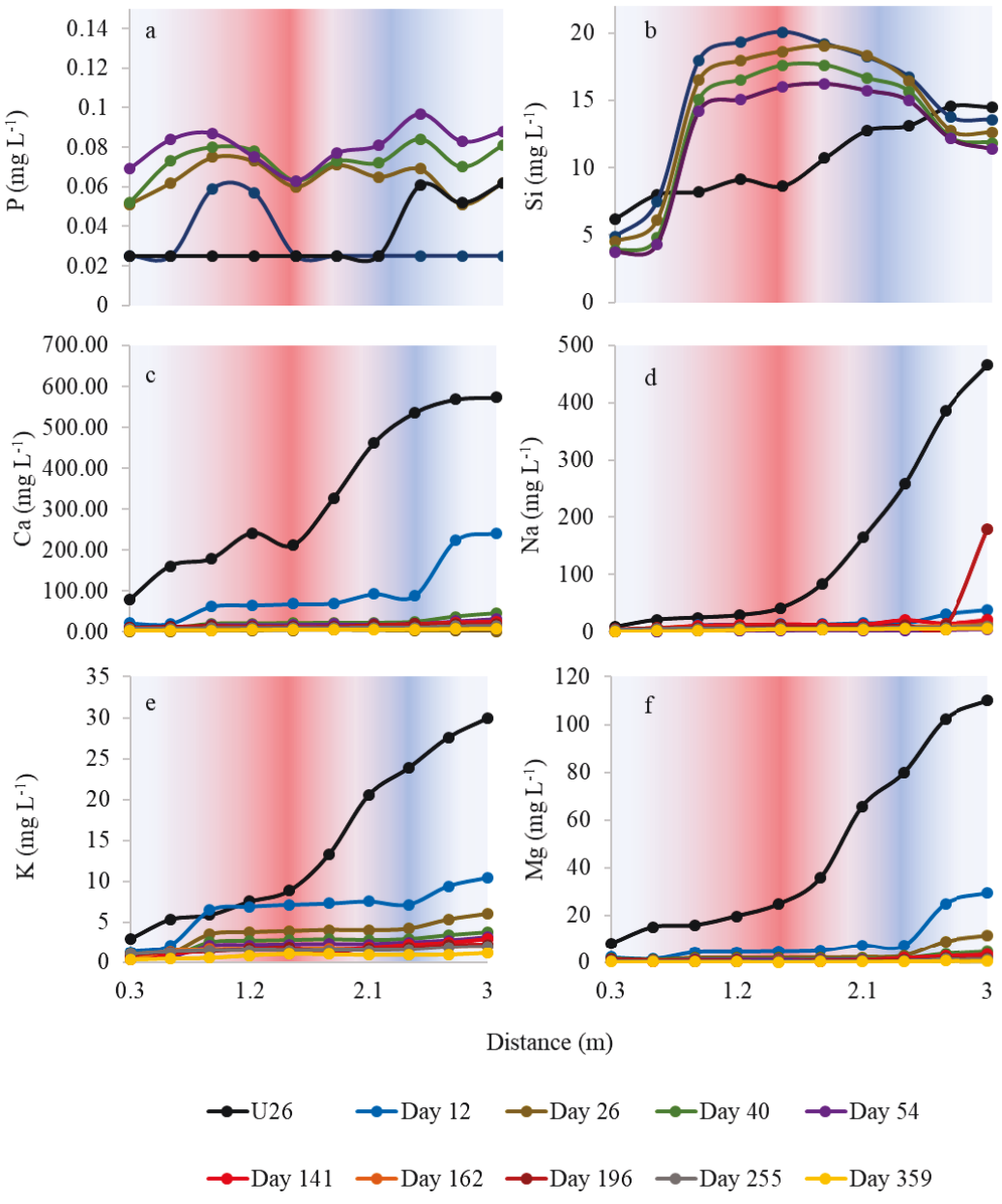


*Figure 4.4 Aqueous concentrations of phosphorous (a), silica (b), calcium (c), sodium (d), potassium (e), and magnesium (f) along the length of the column throughout the sampling period. Any samples that had concentrations <DL were plotted as the DL.*

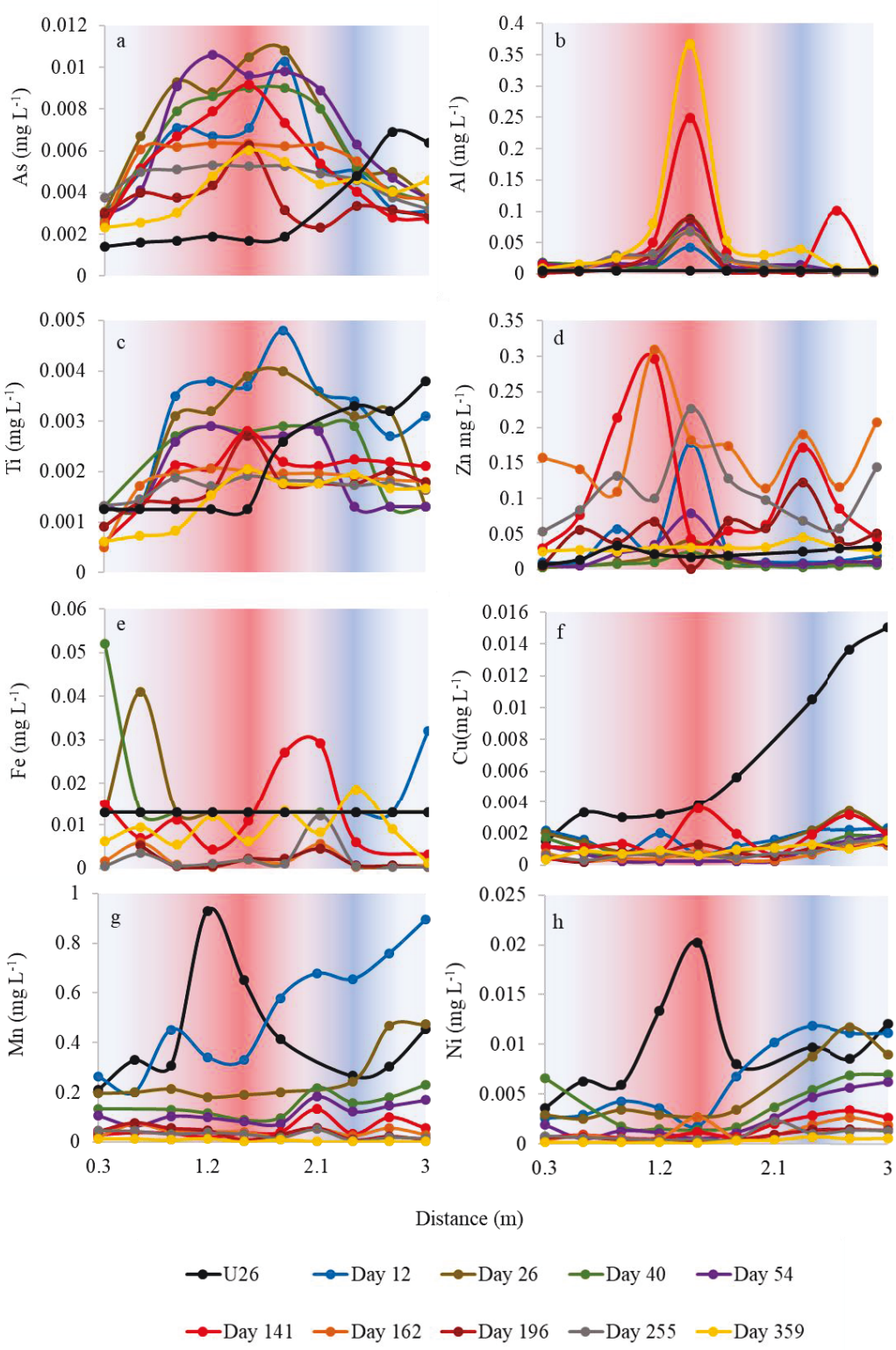


*Figure 4.5 Aqueous concentrations of arsenic (a), aluminum (b), titanium (c), zinc (d), total iron (e), copper (f), manganese (g), and nickel (h) along the length of the column throughout the sampling period. Any samples that had concentrations <DL were plotted as the DL.*

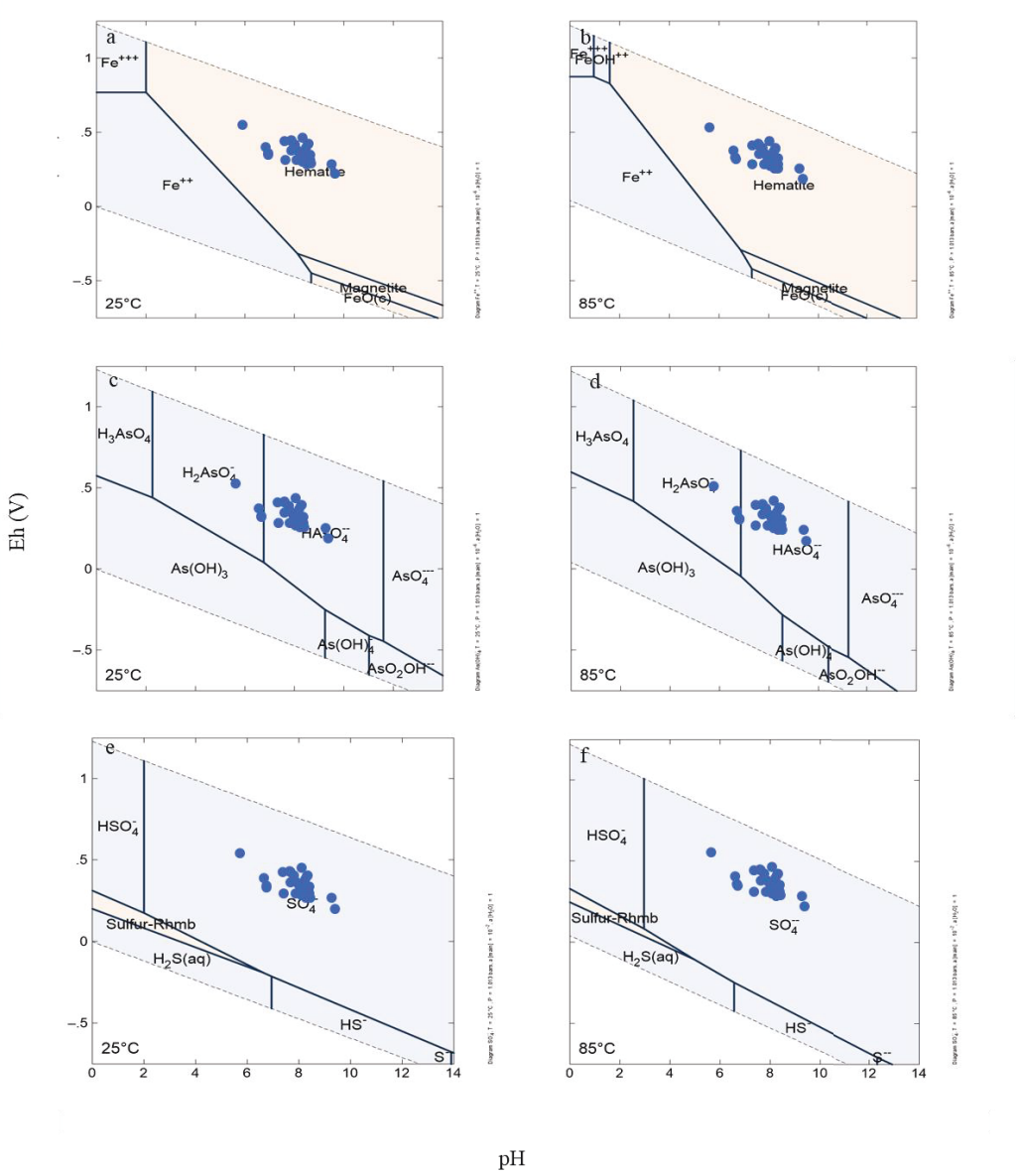


*Figure 4.6 Eh (V) and pH within the column, plotted against phase diagrams of $10^{-5}$ M iron at 25 ° C (a) and 85 °C (b), $10^{-6}$ M arsenic at 25 °C (c) and 85 °C (d), and $10^{-3}$ M sulphate at 25 °C (e) and 85 °C (f). Phase diagrams were constructed using Geochemists Workbench (Bethke & Yeakel, 2009). Blue phases are dissolved species whereas beige phases are solids.*

### 4.1.3 Sediment Characterization

The bulk XRD data acquired on the sediment collected at the end of the heated study indicated a predominance of quartz ($SiO_2$), followed next by feldspar (Na, K ($AlSi_3O_8$); Figure 4.7). The data also indicated a possible presence of phyllosilicates; specifically, clay such as illite (K, Al ($AlSi_3O_{10}$)$(OH)_2$) and/or mica, either as biotite (Al, $Fe^{3+}$, Mg ($Si2O_{10}$)$(OH)_2$) or muscovite (K, $Al_2$ ($AlSi_3O_{10}$)$(FOH)_2$), suggesting they were at a weight percentage (wt %) greater than 5. However, the data is skewed based on the abundance of quartz. The data indicated that this bulk composition of primarily quartz, with feldspar and minor amounts of phyllosilicates, did not change throughout the column. Furthermore, no other minerals were detected using XRD analysis. However, using EMPA, minerals other than those that made up the bulk minerology within the column, while at low concentrations, were observed throughout various sections and are discussed.

Quartz, microcline( $K(AlSi_3O_8)$), and albite ( $Na(AlSi_3O_8)$) were present in all thin sections examined using EMPA/EDS and were the most commonly observed minerals throughout the column (Figure 4.8a-c).The feldspars analyzed contained minor amounts of calcium, iron, magnesium, and/or titanium in addition to silica, aluminum, sodium and/or potassium. These minor elements collectively were found to compose less than 1 wt %. This did not change significantly throughout the column as all of these grains analyzed contained some combination of those minor elements. The grains observed did not change in appearance significantly throughout the column. Unlike the feldspars, the quartz grains observed (like the one depicted in Figure 4.8d) were found to contain minor

amounts of calcium, iron, magnesium, titanium, and/or aluminum, collectively at 0.80 ± 0.20 wt %, but only in sediment from 0.9-2.2 m along the length of the column. Quartz crystals analyzed in sections outside of those sections were relatively pure, containing as little as < 0.10 wt % in the minor elements discussed. One quartz grain, at 2.2 m, was found to contain 0.03 wt % of arsenic (Figure 4.11d).

Oxides were also present, especially iron oxides, which were observed all throughout the column (Figure 4.9a). The form of iron oxides/hydroxides present could not exactly be determined, due to the heterogeneity and soft nature of the material, resulting in analyses lacking in accuracy. Titanium oxides were also observed, however only in sections at 1.5 m, 1.6 m and 2.5 m along the length of the column (Figure 4.9b). Minor amounts of titanium were found in most of the iron oxides analyzed, from as little as 0.25 to as high as 3.17 wt %. Ilmenite ($FeTiO_3$) was found at 1.5 m and 1.6 m along the length of the column. All titanium-rich oxides, including ilmenite, contained manganese, from 5.1-25.6 wt %. The analyses via EMPA further indicated the presence of sheet silicates, as minor amounts of biotite were observed at 1.6 m along the length of the column (Figure 4.9c).

Potential sulphides from 0.2-0.9 m along the length of the column were often too small and too few to analyze by EMPA and were identified as sulphides, likely pyrite, by EDS only. In sediment from 1.1-2.5 m, sulphides were much more plentiful and were most often found in clusters of spherical grains (Figure 4.10a). Many of the sulphide grains contained minor amounts of arsenic, manganese, and/or lead. Arsenic was found in sulphide grains from 1.1-2.9 m along the length of the column, where arsenic ranged

from 0.01-0.35 wt %. Those that contained manganese were found in sections within 0.4-1.6 m and 2.2-2.5 m, where manganese ranged from 0.03-0.24 wt %. Those with lead were found in sections within 1.8-2.9 m, where lead ranged from 0.06-0.20 wt % (Figure 4.10b).

Phosphates were observed in sections 1.1-2.5 m. There were three types of phosphate minerals found; apatite ($Ca_5(PO_4)_3$), an iron phosphate, and an aluminum phosphate (Figure 4.11a-c). The iron and aluminum phosphates were only observed within sediment at 2.2 m along the length of the column and, due to the large portion of unaccounted weight percentage, these grains were likely hydrated (i.e. in the forms of either $Fe_x(PO_4^{2-})_x \cdot xH_2O$ and $Al_x(PO_4^{2-}) \cdot xH_2O$, respectively). However, the aluminum-rich phosphate grain contained a small amount of cerium (Ce), which was not analyzed via EPMA but was detected by EDS, indicating that it was likely monazite-Ce ($CePO_4$) with concentrations of adsorbed hydrolyzed aluminum species. Furthermore, the iron phosphate grain exhibited textures, such as cracks, that suggest it was undergoing dissolution. Apatite was found both within and outside of that section and exhibited no signs of dissolution. No arsenic was found in apatite, but the iron and aluminum-rich phosphates were found to contain arsenic at a range of 0.15-3.51 wt %.

SI for various minerals was calculated using PHREEQC. Silicates were found to exhibit similar trends. During the unheated study (day 0), quartz was undersaturated from 0.3-1.5 m along the length of the column and slightly oversaturated from 1.8-3.0 m (Figure 4.12a). During the heated study (days 12-359), quartz exhibited the similar trends outside of the heated section but, SI dropped sharply within the heated section, at 1.2-1.5 m.

During the unheated study, microcline was oversaturated throughout the entire column (Figure 4.12b). During the heated study, SI for microcline was generally undersaturated within the heated section of the column and oversaturated, or close to saturation, outside of the heated section, with the exception of day 227, where microcline was undersaturated throughout the entire column, except from 2.7-3.0 m along the length of the column. Albite was generally undersaturated throughout the entire columnduring the unheated study (Figure 4.12c). During the heated study, albite was generally undersaturated throughout the entire column. Muscovite exhibited a similar trend as microcline, as it was oversaturated throughout the column in the unheated study; during the heated study SI remained oversaturated within the column except from 1.2-1.5 m along the length of the column, where it was undersaturated (Figure 4.12d).

The two calcitic minerals that were modelled were gypsum and calcite. SI for gypsum was consistently undersaturated during both the unheated and heated studies but, it approached saturation towards the end of the column during the unheated study (Figure 4.12k). $O_{2(g)}$ was consistently undersaturated during both the unheated and heated studies (Figure 4.12l). SI for calcite was found to be oversaturated throughout the entire column during the unheated study (Figure 4.12e). During the heated study, SI for calcite was generally found to be undersaturated at the beginning of the column (up to 0.6 m) then approached saturation within the heated section; it dropped to below saturation in the cooled section and approached saturation again at the end of the column (3.0 m). However, this was not the case during days 141-227, where the SI for calcite was undersaturated throughout the entire column, and during days 26-54, where SI was oversaturated at 1,5 m along the length of the column.

SI for ferrihydrite was oversaturated throughout the entire column during the unheated study and during the heated study, from days 12-141 (Figure 4.12f). At day 176, it was undersaturated throughout the column except at 1.8 m, where it was oversaturated. During day 227 it was undersaturated throughout the column, except at 0.6 m where it was oversaturated. At day 255, SI approached saturation at 0.9 m, and it was oversaturated at 1.5 and 2.1 m. At day 359 SI was undersaturated from 0.3-0.9 m and oversaturated from 1.2-3.0 m along the length of the column. SI for gibbsite, on the other hand, was much less varied. Gibbsite was oversaturated throughout the entire column during the unheated study.

SI for hydroxyapatite was oversaturated throughout the entire column during the unheated study (Figure 4.12h). During the heated study, SI for hydroxyapatite remained oversaturated, except from 1.8-2.4 m along the length of the column, where it generally approached saturation; during days 40 and 54, SI was undersaturated from 1.8-2.4 m. SI for strengite was found to be undersaturated throughout the entire column during the unheated study (Figure 4.12i). During the heated study, SI was generally undersaturated throughout most of the column, but approached saturation at points within the column, generally at 1.5-2.1 m along the length of the column. Vivianite was undersaturated throughout the entire column during both the unheated and heated studies (Figure 4.12j).

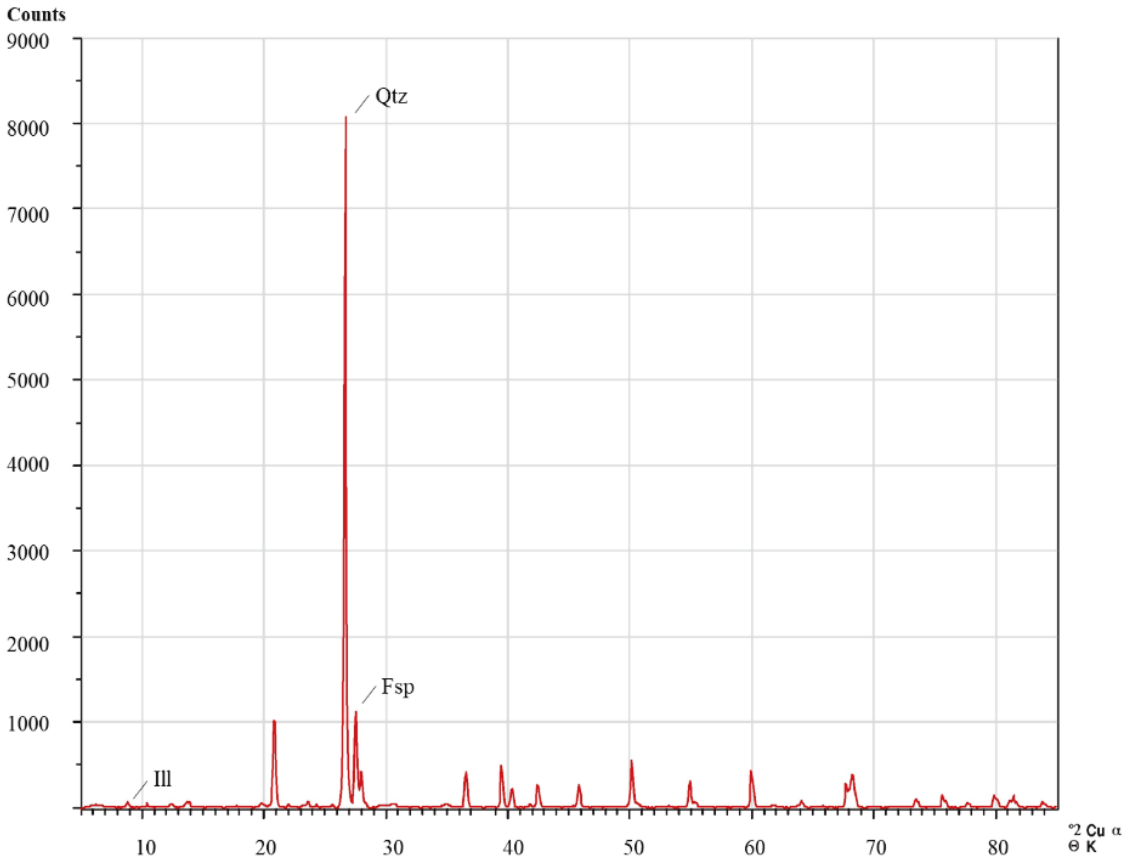


*Figure 4.7 XRD data from section 15. This is representative of the data acquired from all 8 sections.*

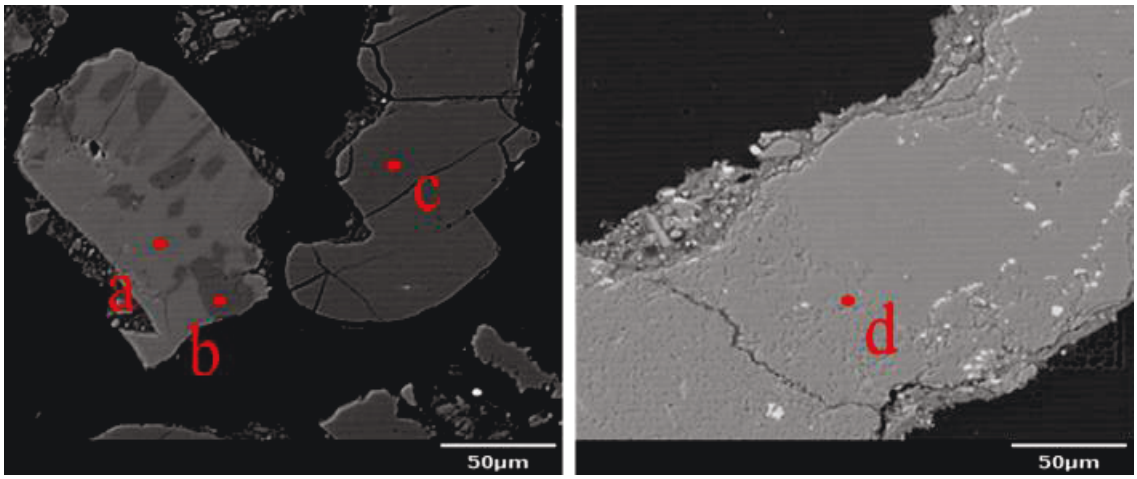


*Figure 4.8 Microprobe images showing microcline (a), albite (b), and quartz (c) in section 4 as well as a quartz grain (d) which was common in sections 9-15.*

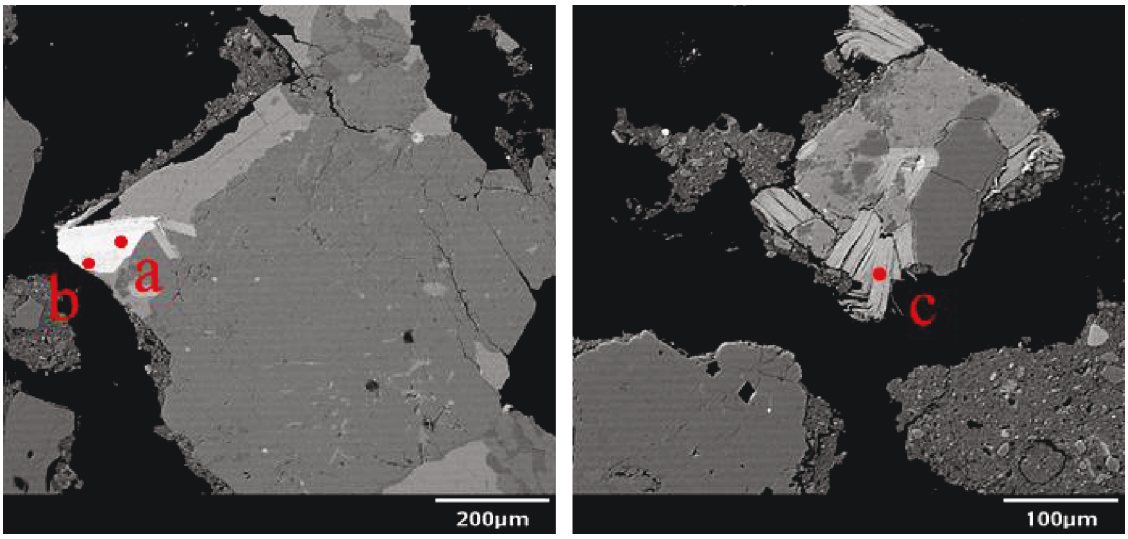


*Figure 4.9 Microprobe images showing an oxide with iron-rich (a) and titanium-rich (b) phases as well as biotite (c). Both were found in section 16.*

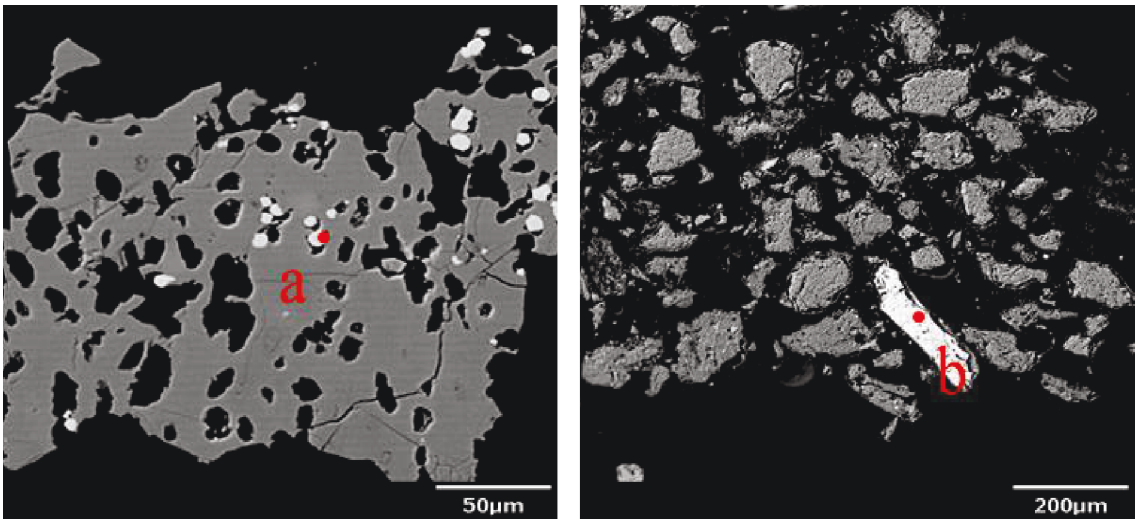


*Figure 4.10 Microprobe images showing pyrite grains in sections 11 (a) and 18 (b). The pyrite cluster observed in section 11 contained minor amounts of manganese whereas the large pyrite grain observed at section 18 contained minor amounts of lead. Both types of grains contained minor amounts of arsenic.*

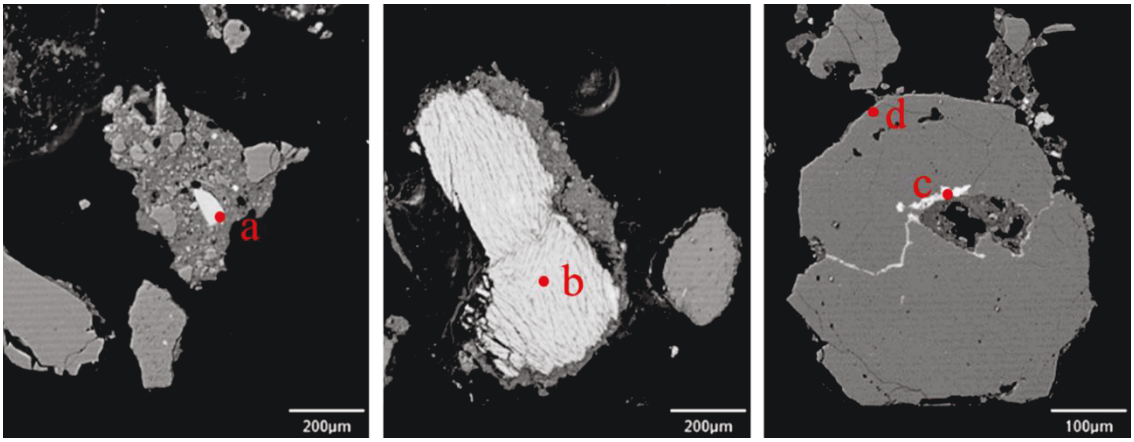


*Figure 4.11 Types of phosphates found within the column including apatite (a), iron-rich (b), and aluminum-rich monazite (c). All three are from section 22. Only the iron and/or aluminum-rich phosphates were found to contain arsenic. Arsenic was also found at the edge of the quartz grain (d).*

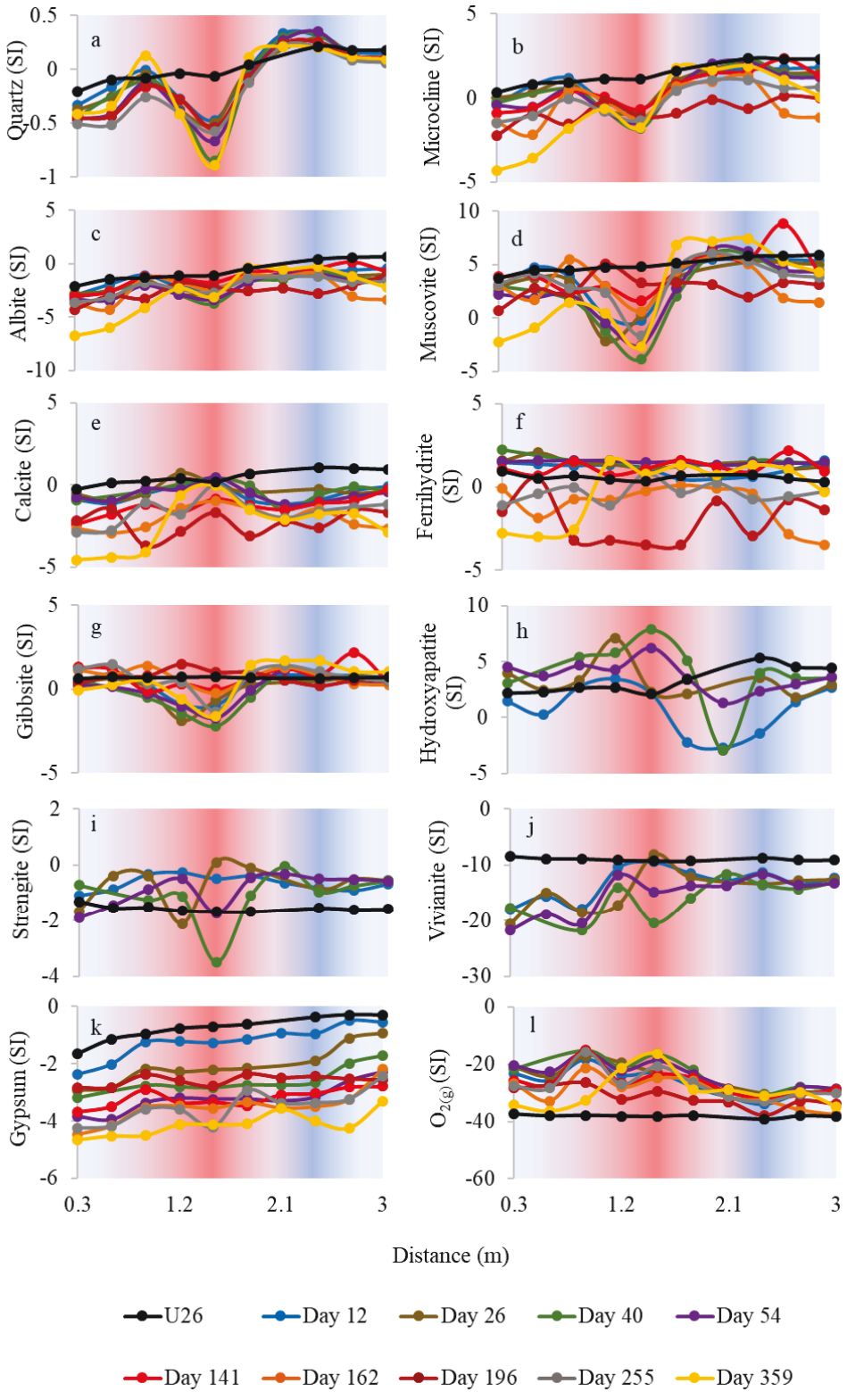


*Figure 4.12 SI for quartz (a), microcline (b), albite (c), muscovite (d), calcite (e), ferrihydrite (f), gibbsite (g), hydroxyapatite (h), strengite (i), vivianite (j), gypsum (k), and $O_{2(g)}$ (l) along the length of the column throughout the study.*

# 5.0 Discussion

## 5.1 Unheated Study

During the unheated study, neither pH nor DO changed significantly throughout the column. The pH was circumneutral while DO ranged from 2.1-3.7 mg $L^{-1}$. However, aqueous concentrations of sulphate, sulphide, and ferrous iron all increased generally from the beginning to the end of the column. This trend was also exhibited by aqueous concentrations of silica and the alkaline/alkali metals calcium, sodium, potassium, and magnesium, which along with sulphate, made up the bulk of the dissolved solids within the column. Aqueous concentrations of phosphorous were generally below the detection limit within the column during the unheated study, except within the last 0.3 m of the column and aqueous concentrations of arsenic were relatively consistent until 1.8 m, where they then began to increase. Aqueous concentrations of copper, like the alkaline/alkali metals, increased along the length of the column.

Spatial trends were not the only trends observed during the unheated study. Some temporal trends were observed as well. Aqueous concentrations of sulphate, sulphide, and the alkaline/alkali metals all generally decreased with increasing number of sampling days. This same trend was generally observed during the heated study as well. The fact that these elements were increasing in concentration with increasing distance along the column, but decreasing with increasing number of sampling days, indicates that flushing of these solutes was occurring. These trends were likely a result of desorption and flushing of products of water-rock interactions that had taken place during the 17-year storage time of the sediment prior to this study.

During storage, water-rock interactions will occur, resulting in the build-up of sulphate, alkaline/alkali metals, and other ions. The trend of increasing concentration with distance generally observed suggests that these ions were being flushed out of the system as DI water was pumped through the column. Surface complexation is likely to have been occurring and a major factor in this. Although sorbents, namely oxide/hydroxides or clays, were not detected via XRD or SEM during the initial geochemical analysis of the sediment, there was evidence of secondary precipitates that indicated a possible presence of iron oxides/hydroxides (Craig, 2017). Furthermore, they were detected in sediment throughout much of the column by EMPA on samples collected at end of the heated study. Unlike the other elements measured in the system, aqueous concentrations of manganese and nickel increased with increasing distance only within the first half of the column. Within the last half of the column, their concentrations decreased with increasing distance along the column. The various trends are likely due to competition for surface sites between different ions.

Sulphides were also not detected via XRD or SEM during the initial geochemical analysis of the column sediment, but digestion of initial sediment samples did indicate concentrations of iron and sulphur greater than 7400 ppm and 380 ppm, respectively (Craig,2017), suggesting there may have been sulphides present but not detected. ICP analysis revealed a spike in aqueous concentrations of manganese, nickel, and sulphate within the first meter of the column during the unheated study, while there was a spike in aqueous concentrations of sulphide within the last meter of the column, suggesting sulphide oxidation may have been occurring, as well as the dissolution of sulphates. SI for gypsum was undersaturated throughout the entire column during the unheated study

but, it did approach saturation towards the end of the column. Sulphate is also known to adsorb to ferrihydrite, and sorption of sulphate, like that of other anions, decreases with increasing pH (Kitadai et al., 2018; Dzombak & Morel, 1990).

## 5.2 Heated Study

During the heated study, some changes were observed within the heated and cooled sections of the column. The pH was acidic-neutral at the beginning and end of the column but was neutral-basic in the heated section of the column. Low pH (< 6.5; particularly at day 227) was likely the result of the low flow rate (< 0.10 mg $min^{-1}$; days 232-241) which was observed during that period of sampling. The range of pH decreased along the length of the column as it was much more varied at the beginning than end of the column. Alkalinity also generally increased along the length of the column, giving evidence as to the ability of the system to buffer itself better at the end of the column than at the beginning. Temporal trends were observed as well. While alkalinity generally increased with increasing distance along the column, it generally decreased with increasing number of sampling days during days 19-47 but, by day 283 it had increased again. The variations in alkalinity were likely due to the fluctuations in flow rate.

The spatial variation in pH within the heated and cooled sections of the column is likely the result of multiple processes. The solubility of both $CO_2$ and calcite has been shown to decrease with increasing temperature (He & Morse, 1993; Larson & Buswell, 1942). Furthermore, the removal of $CO_2$ often results in a pH increase which also affects the solubility of calcite, often leading to its precipitation (Larson & Buswell, 1942). Although calcite was not detected within the heated section via XRD or EMPA at the end

of the heated study, the ICP results, coupled with the calculated SI for calcite, indicate that calcite could have precipitated in the heated section of the column. Aqueous concentrations of calcium increased generally throughout the column, except in the heated section where it remained relatively constant, before increasing again in the cooled section, indicating that multiple processes, resulting in both the release and consumption of calcium, may have been occurring. Furthermore, SI for calcite was generally undersaturated outside of the heated section but approached saturation within the heated section and was even oversaturated during days 26-54, suggesting it could have precipitated within the first few weeks of the study.

A build-up of calcite precipitate could explain the reduced flow rate that was observed during the heated study. Other factors that could affect the flow rate, other than the build-up of calcite, could be changing viscosity and density of the fluid, due to the high temperatures. Tracer tests conducted by Craig (2017) on the column indicated that flow within the column is directly influenced by the higher temperatures within the heated section, which caused increases in dispersion and dispersivity by approximately one to two orders of magnitude. Flow within the heated section of the column also appeared to undergo changes with respect to hydraulic conductivity, as this parameter is inherently linked to viscosity and density of the fluid (Craig, 2017).

Like calcite, aqueous concentrations of sodium, magnesium and potassium also increased throughout the column, except in the heated section where they remained relatively constant, before increasing again in the cooled section. Aqueous concentrations of phosphorous decreased within the heated section and increased within the cooled,

whereas silica, arsenic, aluminum, titanium, and zinc generally increased in the heated section and decreased in the cooled. The changing pH, in combination with the high temperatures within the heated section, was likely the major control of the trends observed during the heated study, as solubility of host minerals and surface complexation are both dependent on pH. Most trace metals occur in solution as cations, which generally become increasingly insoluble as pH increases from acidic-basic, and at near-neutral pH, the solubility of most trace-metal cations is severely limited by precipitation as, or coprecipitation with, an oxide, hydroxide, carbonate or phosphate mineral, or more likely by their strong adsorption to hydrous metal oxides, clay or organic matter (Smedley & Kinniburgh, 2002). The solubility of these minerals is influenced by temperature, as well as pH.

Unlike calcite, the solubility of feldspars increases with temperature within 0-100 ° C (Arnórsson & Stefánsson, 1999) but, the dependence of the dissolution rate of feldspar, such as albite, on temperature is not independent of pH; at a pH above neutral, the dependence of the rate of dissolution on temperature may be greater than at neutral pH (Gruber et al., 2016). While SI calculated using PHREEQC for albite was generally undersaturated throughout the column, SI calculated for microcline was oversaturated throughout most of the column, except within the heated section, where it was undersaturated, suggesting that there is a greater potential for dissolution in the heated section. In the process of feldspar dissolution, alkaline ions such as potassium and sodium are constantly generated and pH gradually increases, resulting in basic conditions over time (Xiao et al., 2018), a process that could further explain the pH increase within the heated section of the column.

Like feldspar, quartz and muscovite solubility increases with temperature (Lammers et al., 2017; Rimstidt, 1997). SI for both minerals, calculated using PHREEQC, were undersaturated within the heated section of the column and generally oversaturated outside of the heated section, suggesting that both could have been dissolving within the heated section. Further evidence of this lies within the data from ICP analysis. ICP data revealed that aqueous concentrations of aluminum increased rapidly within the heated section of the column and decreased rapidly within the cooled. SI calculated for gibbsite during the heated study, like quartz and muscovite, was undersaturated within the heated section of the column and oversaturated outside of it, suggesting it too could have been dissociating in the heated section of the column Aluminum hydrolysis is important in understanding the complex chemistry of aluminosilicates, and its concentrations are generally controlled by the solubility of gibbsite (Baes & Mesmer, 1976). The rapid rise in aqueous concentration of aluminum observed reveals the high sensitivity of gibbsite solubility on pH and temperature, which has been established in other literature (Hitch et al., 1980; Lydersen, 1990).

Surface complexation was also likely a control of the aqueous chemistry within the column during the heated study, as was the case in the unheated study. Since surface complexation is dependent on pH it would have had various influence throughout the column The surface charges of quartz and feldspar would have been predominantly negative within the entire column during the heated study, while the surface charges of iron oxides/hydroxides could have shifted to more negative within the heated section compared to outside the heated section. The sorption of alkaline/alkali metals was likely favoured within the heated section of the column, where pH ranged from neutral-basic,

but anion sorption, such as the sorption of arsenates, was likely favoured outside of the heated section. This is supported by ICP data for the alkaline/alkali metals, which generally increased throughout the column, except in the heated section where they remained relatively constant before increasing again in the cooled section. This suggests that they may have been released there through dissolution of host-minerals but then adsorbed to the surfaces of sorbents, such as iron oxides/hydroxides. This also explains the increase of aqueous arsenic concentrations in the heated section of the column. .

Furthermore, surface complexation could have been indirectly influenced by temperature through its influence on equilibrium and therefore, the tendency for sorbents, such as ferrihydrite, to dissolve, precipitate, or transform. Since metals, phosphates, and sulphates are all known to adsorb to ferrihydrite due to its large surface area (Stumm & Morgan, 1996; Lindsay & Moreno, 1960; Moore et al., 1991; Kitadai et al., 2018; Das et al., 2011) a reduction in ferrihydrite in any way can result in the release of its adsorbed constituents. The transformation of ferrihydrite to goethite and/or hematite results in a reduction of surface area but in nature, this transformation occurs only gradually at neutral pH (Langmuir, 1969). However, this transformation has been showed to occur much more rapidly (from years to days) by increasing temperature from 25 ºC to 50-100 °C (Das et al., 2011). Furthermore, ferrihydrite will dissolve in both acidic and basic conditions, which could explain the random spikes in sulphate concentrations observed throughout the heated study.

Redox conditions also influence iron oxide/hydroxides within the system, and thereby surface complexation. Eh measurements taken during the heated study indicate that

conditions were primarily oxidizing throughout the column during the heated study. Eh did decrease within the heated section of the column, to as low as 0.30 V however, pH within the heated section of the column was consistently basic; conditions resulting in the favour of the oxidized species of iron, arsenic, and sulphate. The decrease in Eh observed within the heated section of the column is likely due to a decrease in DO within the heated section of the column. The concentration of dissolved oxygen in water is affected by multiple factors, including temperature, atmospheric pressure, and ionic strength; specifically, DO solubility decreases with increasing temperature and ionic strength (Rounds, Wilde, & Ritz, 2013). SI calculated for $O_{2(g)}$ did not indicate that DO ever approached saturation or was oversaturated during the experiment but, this may be a result of the high variability with the DO measurements. DO was not always found to decrease within the heated section of the column and measurements were quite varied, likely due to the time sensitivity of those measurements.

## 5.3 Changes in Sediment Composition

Sediment from the Empress Formation has been described during various studies, including that by Parks and Andriashek (2002), Javed and Siddique (2014), and Moncur et al. (2015). The sediment used in this study was also characterized by Craig (2017) before being incorporated into the column. The results by Craig (2017) generally agreed with those from previous studies. Craig (2017) found that the bulk minerology prior to heating included quartz and calcite (CaCO3), with moderate amounts of albite and muscovite, with minor amounts of enstatite ($(Fe,Mg)SiO_3$) and sericite ($KAl2(AlSi_3O_{10})(OH)_2$; Craig, 2017). Neither sulphides nor iron oxides/hydroxides were

detected via XRD or SEM but, digestion of sediment samples conducted prior to heating by Craig (2017) indicate concentrations of iron and sulphur greater than 7400 ppm and 380 ppm, respectively, suggesting there may have been sulphides and/or iron oxides/hydroxides present but not detected.

The results from this study indicated that there were no significant changes in the bulk minerology, either between sections along the column or overall throughout the experiment, except that calcite may have dissolved within the system. Calcite, prior to heating, was detected via XRD (Craig, 2017) but, was not detected within any section of the column via XRD at the end of the heated study, indicating that calcite was at a wt % of less than 5 by the end of the experiment. SI calculated using PHREEQC indicates that calcite was undersaturated throughout the column during most of the heated study, except at 1.5 m where it approached saturation, but that at days 141-196 it was undersaturated throughout the entire column. This suggests that calcite was generally dissolving within the column during the study, and it was likely being depleted.

SI calculated using PHREEQC indicates that the silicates within the column would undergo dissolution, generally within the entire column, with the exception of quartz and microcline, which were generally oversaturated outside of the heated section of the column and undersaturated within the heated section, suggesting dissolution for the two, especially quartz, would occur within the heated section of the column. SI calculated for the other silicates, including albite and muscovite, suggests that they may have precipitated outside of the heated section during different periods of the study, likely varying with pH and flow rate, but that in general they would undergo dissolution

throughout the column. The breakdown of these minerals throughout the study would have led to the release of their constituents.

Many oxides/hydroxides, especially iron oxides/hydroxides, as well as sulphides were detected during analysis via EMPA at the end of the study. While none were detected during sediment characterization prior to the heated study, it is likely that they were present but did not make-up a significant wt %. Considering their abundance during the sediment characterization after the heated study, it may be deduced that oxides/hydroxides precipitated at times. Weathering of sheet silicates, such as biotite, can result in the formation of secondary minerals, such as iron (hydr)oxide (Stumm & Morgan, 1996). SI calculated using PHREEQC indicates that ferrihydrite was generally oversaturated, with the exception of the last few sampling days, where it was undersaturated at various sampling sections along the column, likely a response to varying DO.

While no phosphate minerals were detected during the geochemical analyses conducted prior to this study, apatite, an iron phosphate, and an aluminum phosphate (likely monazite) were detected using EMPA at the end of this study. In particular, the iron and aluminum phosphates were detected within the cooled section of the column, while apatite was found within the heated and cooled sections. This could suggest that precipitation of the iron and aluminum phosphates occurred in the cooled section of the column. Calcite can convert to apatite at a pH of 8 (Stumm & Morgan, 1996) but in neutral-acidic conditions, phosphate is thought to be controlled by iron and aluminum concentrations, as strengite and variscite ($AlPO_4 \cdot 2(H_2O)$) are thought to control aqueous

phosphate concentrations in acidic conditions (Stumm & Morgan, 1996; Lindsay & Moreno, 1960; Moore et al., 1991).

SI calculated using PHREEQC indicates that the water in the column was oversaturated with respect to hydroxyapatite within the column during the heated study, but that SI approached saturation from 1.8-2.4 m, and was undersaturated within the cooled section of the column during the beginning of the heated study (days 12-26). SI for strengite was generally undersaturated throughout the column but, approached saturation from 1.5-2.1 m during the beginning of the heated study (days 26-40). Furthermore, while aqueous concentrations of phosphorous were not measured throughout the entire study, ICP-OES data acquired from Craig (2017) show aqueous concentrations of phosphorous decreased in the heated section of the column and increased within the cooled section of the column during the heated study (days 12-54). Aqueous concentrations of total iron were also elevated in the cooled section of the column.

Although no phosphate minerals were detected prior to the study, phosphorous made up a relatively significant portion of the chemical make-up of the sediment (200 ± 55 ppm; Craig, 2017). This suggests that phosphates were present in the original sediment, but at a wt % too low to detect. Therefore, it is more plausible that the iron and aluminum phosphates did not precipitate during the heated study but were pre-existing. The cracks within the iron phosphate grain suggests this to be the case. The dissolution, rather than precipitation, of these minerals also explains the trends in aqueous concentrations of iron and phosphorous that were observed. The dissolution of the iron phosphate could have contributed to the release of iron and phosphorous, resulting in the elevated

concentrations of both elements in the cooled section of the column.

## 5.4 The Release, Mobilization, and Attenuation of Arsenic

No sources of arsenic were detected via XRD or EMPA in the first 0.8 m of the column. However, arsenic was detected in sulphides from 0.9-2.9 m along the length of the column and therefore, sulphides are thought to be likely sources of arsenic in this study. Although arsenic was only detected via EMPA in sediment between 0.9-2.9 m along the length of the column, it is likely that it was present within sulphides from 0.3-0.9 m along the length of the column, but at a wt % too low to detect. Arsenic would have been redistributed from the beginning of the column towards the end of the column, due to its release from sediment in the heated section of the column to sediment within the cooled section of the column. It is likely there were other sources and/or sinks of arsenic in the column, such as aluminosilicates and oxides/hydroxides. However, any arsenic that may have been present within any of those minerals, if any, was at a wt % too low to detect.

Aqueous concentrations of arsenic increased in the heated section of the column, to concentrations above the MAC, and decreased in the cooled section of the column, to concentrations below the MAC, during the first 54 days of the heated study. Afterwards, arsenic concentrations never exceeded the MAC but, concentrations did still generally increase within the heated section of the column and decrease within the cooled. Other elements that exhibited this trend of increasing in the heated section and decreasing in the cooled section included aluminum, titanium and zinc. One possibility for this trend is that arsenic was desorbing from oxidized forms of these metals, such as gibbsite, which would dissociate in the heated section due to the high pH that was apparent. However,

aqueous concentrations of arsenic rose much more slowly and fell much more slowly, within the heated and cooled sections, than aluminum. Therefore, it is more likely that the release of arsenic was due to a combination of processes, including: 1) dissolution of host-minerals and sorbents, of which arsenic would be released or desorbed from, 2) redox conditions, or 3) changing pH.

Specific processes that can result in the release of arsenic into the groundwater system include arsenic-bearing mineral dissolution and desorption of arsenic from soil and/or carbonate material or iron, aluminum, and/or manganese oxides (Lemay, 2003). While the data from this study indicates that calcite may have precipitated within the heated section of the column, the solubility of aluminosilicates generally would have increased within the heated section, which could have contributed to the release of arsenic. The transformation of ferrihydrite to goethite and/or hematite, resulting in a reduction of surface area (Dzombak & Morel, 1990) which would reduce its ability to adsorb arsenic, could also contribute to the release of arsenic within the heated section, where temperature was high enough to induce this transformation.

The form of arsenic prevalent in the system is also important. Under reducing conditions, arsenite is prevalent and more mobile than arsenate. However, this system was oxidized, and arsenic was likely in the form of arsenate. While less mobile in general, its mobility is heavily influenced by pH. Therefore, it is more likely that pH was the major control of aqueous concentrations of arsenic. pH not only influences the species of arsenic present but, pH also influences the affinity for adsorption of arsenate, specifically. While conditions may not have been reducing enough for the prevalence of arsenite, the

increase of pH from neutral-basic was likely high enough to increase mobility of arsenic in the arsenate form, since oxyanions of arsenate tend to become less strongly sorbed as pH increases (Dzombak & Morel, 1990), even at near-neutral pH values (Smedley & Kinniburgh, 2002). Furthermore, the rate of desorption of arsenic would likely have increased as temperature increased, since reaction rates in general increase with increasing temperature (Langmuir, 1997).

Outside of the heated section, aqueous concentrations of arsenic decreased slowly, suggesting that attenuation did not happen rapidly. The decrease in pH within the cooled section of the column, from basic-neutral (and from neutral-basic at times) was likely a control on the attenuation of arsenic. At neutral pH, the affinity of arsenic for sorption is at a maximum, increasing with decreasing pH. Although no arsenic was detected via EMPA in association with any iron oxides/hydroxides that were present, it was detected along the edge of one quartz grain within the cooled section of the column, suggesting attenuation of arsenic did occur via adsorption. Arsenic was also detected within iron and aluminum phosphates, suggesting that iron, aluminum, and phosphate concentrations were also controls on arsenic attenuation, through surface complexation and/or co-precipitation. Both amorphous and crystalline iron (III) phosphate are efficient at arsenic removal through arsenate/phosphate substitution (Lenoble, Laclautre, Deluchat, Serpaud, & Bollinger, 2005), where the tetrahedral $AsO_4^{3+}$ arsenate group substitutes for the tetrahedral $PO_4^{3-}$ phosphate group (Pan & Fleet, 2002; Lee et al., 2009; Zhu et al., 2009).

# 6.0 Conclusion

The results of this study demonstrated the long-term effects of thermal recovery operations on the release, mobilization, and attenuation of arsenic in groundwater, as well as its influence on water quality in general. The results demonstrated that temperatures from 50-90 °C have the potential to release contaminants, such as arsenic, titanium, aluminum, and zinc, by influencing mineral solubility and surface complexation. Most importantly, the results of this study demonstrate the influence of pH, where the increase and decrease of pH seems to greatly influence mobility of metals in a system impacted by thermal recovery operations by influencing dissolution and precipitation of minerals and by controlling surface complexation. Surface complexation, specifically the competition for surface sites between ions, seems to have been the major control on the release and mobility of arsenic during this study.

The influence of temperature on adsorption is not clear cut; temperature will increase the rate of adsorption, since reaction rate in general increases with increasing temperature. However, this will only be the case if adsorption is favoured thermodynamically; its role is dependent on pH. In the case of arsenic, desorption is favoured in basic conditions, and this is what was observed within this system. The release of arsenic seems to have been controlled by increasing/decreasing pH and was possibly influenced further by increasing/decreasing temperature. However, this may not have been the case if pH did not increase from neutral-basic within the heated section of the column, so this phenomenon depends greatly on other factors controlling the system, namely buffers such as calcite. Furthermore, the results of this study demonstrate the relationship between

arsenic, iron, aluminum, and phosphate.

Within this system, the original source of arsenic may not have been determined, but it is believed that arsenic was originally within the column as a sulphide or adsorbed to oxide/hydroxides. The detection of arsenic within sulphide grains from 0.9-2.9 m along the length of the column at the end of the heated study presents some evidence that this could be the case. While the original source of arsenic could not be determined, phosphate was determined to be a sink for arsenic. The detection of arsenic within iron and aluminum-rich phosphate grains suggests these are sinks for arsenic within this system and shows the ability for arsenic to attenuate outside of heated zones by adsorbing to or co-precipitating with these minerals. Furthermore, despite arsenic making up a very minor amount of the sediment within the column (generally < 5 ppm within samples of the sediments; Craig, 2017) aqueous concentrations of arsenic were still driven above the MAC within the heated section of the column during the first 54 days of the heated study.

Further insight into the controlling mechanisms of arsenic release, mobilization, and attenuation in systems adjacent to thermal recovery operations could be complimented by developing a reactive transport model. Additionally, further column experiments could be conducted using higher temperatures as well as using various sediment samples from multiple aquifer units within the Oil Sands In-Situ Area, since various aquifer units within the area do have high background arsenic concentrations (> 30 ppm, compared to < 5 ppm within the sediment used in this study), which could have even greater implications on the release of arsenic. Furthermore, the varying geochemistry of the different units within the area could affect the behaviour of arsenic in different ways; it is

crucial to implement studies involving different units to understand the long-term effects of thermal recovery operations on the release, mobilization, and attenuation of arsenic.

# 7.0 References

Canadian Natural Resources Limited [CNRL] (2006). *Primrose East Expansion Project Application for Approval to Alberta Energy and Utilities Board and to Alberta Environment*.

Allison, J. d., Brown, D. S., & Novo-gradac, K. J. (1991). MINTEQA2/PRODEFA2, a Geochemical Assessment Model for Environmental Systems: version 3. *0 User's Manual. Environmental Research Laboratory, Office of Research and Development, USEPA*, (January 1991).

Appelo, C. A. J., & Postma, D. (2005). *GEOCHEMISTRY, GROUNDWATER AND POLLUTION* (second). Amsterdam, Netherlands: A.A. Balkema Publishers.

Baes, C. F., & Mesmer, R. E. (1976). *The Hydrolysis of Cations*. New York: Wiley-Interscience.

Boyle, R. W., & Jonasson, I. R. (1973). the Geochemistry of Arsenic and Its Use As an Indicator. *Journal of Geochemical Exploration*, *2*, 251–296. https://doi.org/10.1016/0375-6742(73)90003-4

Canadian Association of Petroleum Producers [CAPP] (2018). Recovering the Oil. Retrieved from What are the oil sands? website: http://www.canadasoilsands.ca/en/what-are-the-oil-sands/recovering-the-oil

Canadian Water Network [CWN] (2015). Arsenic in Canadian Drinking Water. Retrieved

from http://cwn-rce.ca/wp-content/uploads/2015/04/ChrisLe-Arsenic-in-Canadian-Drinking-Water-Full-Report-2014.pdf

Craig, A. (2017). *Using heated column experiments to investigate the effects of in-situ thermal recovery operations on groundwater geochemistry in Cold Lake, Alberta*. Carleton University.

Das, S., Hendry, M. J., & Essilfie-Dughan, J. (2011). Transformation of two-line ferrihydrite to goethite and hematite as a function of pH and temperature. *Environmental Science and Technology*, *45*(1), 268–275. https://doi.org/10.1021/es101903y

Dzombak, D. A., & Morel, F. M. M. (1990a). *Surface Complexation Modeling: Hydrous Ferric Oxide*. New York: John Wiley and Sons Inc.

Dzombak, D. A., & Morel, F. M. M. (1990b). *Surface complexation modelling – hydrous ferric oxide*. New York, New York: John Wiley.

Fennell, J. (2008). *Effects of Aquifer Heating on Groundwater Chemistry with a Review of Arsenic and its Mobility*. The Univeristy of Calgary.

Giraldo, N. M., & MacMillan, G. (2016). *Temperature Plume Migration in Aquifers: The necessary first step to geochemical evaluation of thermally-mobilized constituents.* Calgary, Alberta.

Government of Alberta [GOA] (2017). Steam Assisted gravity drainage facts and stats.

Retrieved from https://open.alberta.ca/dataset/f7c779ea-9776-4d59-a1b3-178d533f0ebc/resource/aac73d46-3ae0-478e-9b19-e64afa41b1f2/download/FSSAGD.pdf

Government of Alberta [GOA] (2019). The Location of oil sands. Retrieved from http://history.alberta.ca/energyheritage/sands/origins/the-geology-of-the-oil-sands/the-location-of-oil-sands.aspx

Government of Canada [GOC]. (2013). Groundwater. Retrieved from http://www.ec.gc.ca/eau-water/default.asp?lang=En&n=300688DC-1%A0

Health Canada. (2006). *Guidelines for Canadian Drinking Water Quality: Guideline Technical Document*.

Hitch, B. F., Mesmer, R. E., Baes, C. F., & Sweeton, F. H. (1980). The solubility of (a-Al(OH)3) in 1 molal NaCl as a function of pH and temperature. *Oak Ridge National Laboratory Report ORNL-5623*.

Javed, M. B., Kachanoski, G., & Siddique, T. (2014). Arsenic fractionation and mineralogical characterization of sediments in the Cold Lake area of Alberta, Canada. *Science of the Total Environment*, *500–501*, 181–190. https://doi.org/10.1016/j.scitotenv.2014.08.083

Javed, M. B., & Siddique, T. (2016). Thermally Released Arsenic in Porewater from Sediments in the Cold Lake Area of Alberta, Canada. *Environmental Science and Technology*, *50*(5), 2191–2199. https://doi.org/10.1021/acs.est.5b04555

Kitadai, N., Nishiuchi, K., & Tanaka, M. (2018). A comprehensive predictive model for sulfate adsorption on oxide minerals. *Geochimica et Cosmochimica Acta*, *238*(1), 150–168.

Lammers, K., Smith, M. M., & Carroll, S. A. (2017). Muscovite dissolution kinetics as a function of pH at elevated temperature. *Chemical Geology*, *466*(June), 149–158. https://doi.org/10.1016/j.chemgeo.2017.06.003

Langmuir, D. (1997). *Aqueous Environmental Geochemistry*. Englewood Cliffs: Prentice-Hall, Inc.

Lee, Y. J., Stephens, P. W., Tang, Y., Li, W., Phillips, B. L., Parise, J. B., & Reeder, R. J. (2009). Arsenate substitution in hydroxylapatite: structural characterization of the Ca5(PxAs1–xO4)3OH solid solution. *Am. Mineral.*, *94*, 666–675.

Lemay, T. G. (2003). *Arsenic Concentrations in Quaternary Drift and Quaternary-Tertiary Buried Channel Aquifers in the Athabasca Oil Sands (In Situ) Area, Alberta*.

Lenoble, V., Laclautre, C., Deluchat, V., Serpaud, B., & Bollinger, J. C. (2005). Arsenic removal by adsorption on iron(III) phosphate. *Journal of Hazardous Materials*, *123*(1–3), 262–268. https://doi.org/10.1016/j.jhazmat.2005.04.005

Lindsay, W. L., & Moreno, E. C. (1960). Phosphate phase equilibriums in soils. *Soil Science Society of America Proceedings*, *24*(3).

Lydersen, E. (1990). The solubility and hydrolysis of aqueous aluminium hydroxides in dilute fresh waters at different temperatures. *Nordic Hydrology*, *21*(3), 195–204. https://doi.org/10.2166/nh.1990.0015

Moncur, M. C., Paktunc, D., Jean Birks, S., Ptacek, C. J., Welsh, B., & Thibault, Y. (2015). Source and distribution of naturally occurring arsenic in groundwater from Alberta's Southern Oil Sands Regions. *Applied Geochemistry*, *62*, 171–185. https://doi.org/10.1016/j.apgeochem.2015.02.015

Moore, P. A., Jr; Reddy, K. R., & Graetz, D. A. (1991). Phosphorus geochemistry in the sediment-water column of a hypereutrophic lake. *Journal of Environmental Quality*, *20*(4), 869–865.

Muloin, T., & Dudas, M. J. (2011). Aqueous phase arsenic in weathered shale enriched in native arsenic. *Journal of Environmental Engineering and Science*, *4*(6), 461–468.

Natural Resources Canada [NRC] (2018). Crude Oil Facts. Retrieved from https://www.nrcan.gc.ca/energy/facts/crude-oil/20064

Pan, Y. M., & Fleet, M. E. (2002). Compositions of the apatite-group minerals: substitution mechanisms and controlling factors. *Rev. Mineral. Geochem.*, *48*, 13–49.

Parkhurst, D. L., & Appelo, C. A. J. (2013). *Description of input and examples for PHREEQC version 3 – A Computer Program for Speciation, Batch-reaction, One-Dimensional Transport, and Inverse Geochemical Calculations*.

Parks, K., & Andriashek, L. D. (2002). *Baseline Investigations into the Groundwater Resources of the Athabasca Oil Sands (In Situ) Area, Northeast Alberta*.

Porro, I., Newman, M. E., & Dunnivant, F. M. (2000). Comparison of batch and column methods for determining strontium distribution coefficients for unsaturated transport in basalt. *Environmental Science and Technology*, *34*(9), 1679–1686. https://doi.org/10.1021/es9901361

Rounds, S. A., Wilde, F. D., & Ritz, G. F. (2013). *Dissolved oxygen (ver. 3.0): U. S. Geological Survey Techniques of WaterResources Investigations, book 9, chap. A6, sec. 6.2*. Retrieved from http://water.usgs.gov/owq/FieldManual/Chapter6/6.2_v3.0.pdf

Smedley, P. L., & Kinniburgh, D. G. (2002). A review of the source, behaviour and distribution of arsenic in natural waters. *Applied Geochemistry*, *17*(5), 517–568. https://doi.org/10.1016/S0883-2927(02)00018-5

Smith, A. H., Lingas, E. O., & Rahman, M. (2000). Contamination of Drinking Water by Arsenic in Bangladesh : A Public Health Emergency . Bulletin of the World Health Organization 78 : Contamination of drinking-water by arsenic in Bangladesh : a public health emergency. *World Health Organization. Bulletin of the World Health Organization*, *78*(August 2016), 1093. https://doi.org/10.1590/S0042-96862000000900005

Stumm, W., & Morgan, J. J. (1996). *Aquatic chemistry: Chemical equilibria and rates in natural waters.* New York: Wiley.

Waterline Inc. (2011). *Kirby In-Situ Oil Sands Project Hydrogeology Baseline*.

Welch, A. H., Lico, M. S., & Hughes, J. L. (1988). Arsenic in ground water of the Western United States. *Groundwater*, *26*(3), 333–347.

World Health Organization [WHO]. (2011). Arsenic Fact Sheet. Retrieved from https://www.who.int/news-room/fact-sheets/detail/arsenic

Zhu, Y., Zhang, X., Long, F., Liu, H., Qian, M., & He, N. (2009). Synthesis and characterization of arsenate/phosphate hydroxyapatite solid solution. *Mater. Lett.*, *63*, 1185–1188.